Modulation of dopamine D_1 receptors via histamine H_3 receptors is a novel therapeutic target for Huntington's disease

David Moreno-Delgado[1,2†‡], Mar Puigdellívol[2,3,4,5†§], Estefanía Moreno[1,2], Mar Rodríguez-Ruiz[1,2], Joaquín Botta[1,5], Paola Gasperini[5], Anna Chiarlone[2,6], Lesley A Howell[7], Marco Scarselli[8], Vicent Casadó[1,2], Antoni Cortés[1,2], Sergi Ferré[9], Manuel Guzmán[2,6], Carmen Lluís[1,2], Jordi Alberch[2,3,4], Enric I Canela[1,2], Silvia Ginés[2,3,4†*], Peter J McCormick[1,2,5,10†*]

[1]Department of Biochemistry and Molecular Biomedicine, Faculty of Biology, Institute of Biomedicine of the University of Barcelona (IBUB), University of Barcelona, Barcelona, Spain; [2]Centro de Investigación Biomédica en Red sobre Enfermedades Neurodegenerativas, Madrid, Spain; [3]Department of Biomedical Science, Faculty of Medicine, University of Barcelona, Institut of Neuroscience, Barcelona, Spain; [4]Institut d'Investigacions Biomèdiques August Pi i Sunyer (IDIBAPS), Barcelona, Spain; [5]School of Pharmacy, University of East Anglia, Norwich Research Park, Norwich, United Kingdom; [6]Department of Biochemistry and Molecular Biology I, School of Biology, Instituto Universitario de Investigación Neuroquímica, and Instituto Ramón y Cajal de Investigación Sanitaria, Complutense University of Madrid, Madrid, Spain; [7]School of Biological and Chemical Sciences, Queen Mary University of London, London, United Kingdom; [8]Department of Translational Research and New Technologies in Medicine and Surgery, University of Pisa, Pisa, Italy; [9]National Institute on Drug Abuse, Intramural Research Program, National Institutes of Health, Department of Health and Human Services, Baltimore, United States; [10]William Harvey Research Institute, Barts and the London School of Medicine, Queen Mary University of London, London, United Kingdom

*For correspondence:
silviagines@ub.edu (SG);
p.mccormick@qmul.ac.uk (PJMC)

†These authors contributed equally to this work

Present address: ‡UCB BioPharma SPRL, Chemin de Foriest, Braine-l'Alleud, Braine-l'Alleud, Belgium; §Department of Biochemistry, University of Cambridge, Cambridge, United Kingdom

Abstract Early Huntington's disease (HD) include over-activation of dopamine D_1 receptors (D_1R), producing an imbalance in dopaminergic neurotransmission and cell death. To reduce D_1R over-activation, we present a strategy based on targeting complexes of D_1R and histamine H_3 receptors (H_3R). Using an HD mouse striatal cell model and HD mouse organotypic brain slices we found that D_1R-induced cell death signaling and neuronal degeneration, are mitigated by an H_3R antagonist. We demonstrate that the D_1R-H_3R heteromer is expressed in HD mice at early but not late stages of HD, correlating with HD progression. In accordance, we found this target expressed in human control subjects and low-grade HD patients. Finally, treatment of HD mice with an H_3R antagonist prevented cognitive and motor learning deficits and the loss of heteromer expression. Taken together, our results indicate that D_1R - H_3R heteromers play a pivotal role in dopamine signaling and represent novel targets for treating HD.

Introduction

Huntington's disease (HD) is a dominant inherited progressive neurodegenerative disorder caused by expansion of a CAG repeat, coding a polyglutamine repeat within the *N*-terminal region of huntingtin protein (*Macdonald, 1993*; *Vonsattel and DiFiglia, 1998*). Although dysfunction and death of striatal medium-sized spiny neurons (MSSNs) is a key neuropathological hallmark of HD (*Ferrante et al., 1991*; *Vonsattel et al., 1985*), cognitive deficits appear long before the onset of motor disturbances (*Lawrence et al., 2000*; *Lemiere et al., 2004*). It has been postulated that alterations in the dopaminergic system may contribute to HD neuropathology (*Chen et al., 2013a*; *Jakel and Maragos, 2000*), as dopamine (DA) plays a key role in the control of coordinated movements. Increased DA levels and DA signaling occur at early stages of the disease (*Chen et al., 2013a*; *Garret et al., 1992*; *Jakel and Maragos, 2000*), resulting in an imbalance in striatal neurotransmission initiating signaling cascades that may contribute to striatal cell death (*Paoletti et al., 2008*; *Ross and Tabrizi, 2011*). Several studies demonstrated that DA receptor antagonists and agents that decrease DA content reduce chorea and motor symptoms while dopaminergic stimulation exacerbate such symptoms (*Huntington Study Group, 2006*; *Mestre et al., 2009*; *Tang et al., 2007*).

Within the striatum, two different MSSNs populations can be distinguished: 1) MSSNs expressing enkephalin and dopamine D_2 receptors (D_2R), which give rise to the indirect striatal efferent pathway, and 2) MSSNs expressing substance P and dopamine D_1 receptors (D_1R), comprising the direct striatal efferent pathway. Recently, several studies with experimental models have changed the traditional view that D_2R-MSSNs are more vulnerable in HD (*Cepeda et al., 2008*; *Kreitzer and Malenka, 2007*), proposing a new view in which D_1R-MSSNs are more vulnerable to the HD mutation. In this view, it has been demonstrated that mutant huntingtin enhances striatal cell death through the activation of D_1R but not D_2R (*Paoletti et al., 2008*). More recently, it has been described that, at early stages of the disease, HD mice show an increase in glutamate release onto D_1R neurons but not D_2R neurons while, later in the disease, glutamate release is selectively decreased to D_1R cells (*André et al., 2011a*), indicating that several changes occur in D_1R neurons at both early and late disease stages. Strategies that might reduce D_1R signaling could prove successful towards preventing HD (*André et al., 2011a*; *André et al., 2011b*; *Ross and Tabrizi, 2011*; *Tang et al., 2007*). However, D_1Rs are highly expressed in many tissues (*Beaulieu and Gainetdinov, 2011*) and broad use of D_1R antagonists as a preventive treatment has important drawbacks including locomotor impairments (*Giménez-Llort et al., 1997*), or induce depression, parkinsonism and sedation in HD patients (*Frank et al., 2008*; *Huntington Study Group, 2006*).

Histamine is an important neuromodulator with four known G protein-coupled receptors (GPCRs). H_3Rs are expressed in brain regions involved in both motor function (striatum) and cognition, such as the cortex, thalamus, hypothalamus, hippocampus and amygdala (*Panula and Nuutinen, 2013*). It is known that in at least striatal GABAergic dynorphinergic neurons (*Pillot et al., 2002*; *Ryu et al., 1994a*; *Ryu et al., 1994b*), both D_1R and H_3R are co-expressed and we and others have found that they establish functional negative interactions by forming molecular complexes termed heteromers (*Moreno et al., 2011*; *Sánchez-Lemus and Arias-Montaño, 2004*). Hence, in this work, we hypothesized that targeting D_1R through these receptor complexes of D_1R and H_3R might serve as a more efficient and targeted strategy to slow the progression of HD. Specifically, we demonstrate that D_1R-H_3R heteromers are expressed and functional in early HD stages but are lost in late stages. An H_3R antagonist acting through D_1R-H_3R heteromers acts as a protective agent against dopaminergic imbalance in early HD stages improving learning and long-term memory deficits and rescuing the loss of D_1R-H_3R complexes at late stages of HD.

Results

Functional D_1R-H_3R heteromers are expressed in wild type STHdh^{Q7} and HD STHdh^{Q111} striatal cell models

To test whether D_1R-H_3R heteromers could indeed be targets for controlling D_1R signaling in HD, we first analyzed the expression of both receptors in immortalized striatal cells expressing endogenous levels of full-length wild-type STHdh^{Q7} or mutant STHdh^{Q111} huntingtin (*Ginés et al., 2010*). Ligand binding determined that both STHdh^{Q7} and STHdh^{Q111} cells endogenously express similar

levels of D_1R and H_3R (*Supplementary file 1*). By proximity ligation assays (PLA), D_1R-H_3R heteromers were detected as red spots surrounding the blue stained nuclei in both cell types (*Figure 1A*, left panels of both cell types) and in cells treated with control lentivirus vector (*Figure 1—figure supplement 1A*) but not in cells depleted of H_3R (*Figure 1A*, right panels of both cell types) by shRNA, as shown by RT-PCR and functionality (*Figure 1—figure supplement 1B,C*), or in negative controls (*Figure 1—figure supplement 1D*). To ensure that D_1R-H_3R heteromers were functional in STHdh cells, cell signaling experiments were performed. Using both STHdh^{Q7} and STHdh^{Q111} cells and concentrations of ligands previously shown to be optimal for receptor activation of the ERK1/2 pathway (*Ferrada et al., 2009*; *Moreno et al., 2014*; *Moreno et al., 2011*), we observed that the D_1R agonist SKF 81297 was able to increase ERK1/2 phosphorylation whereas it was prevented by D_1R antagonist SCH 23390, and by the H_3R antagonist thioperamide (*Figure 1—figure supplement 2A, B*) via cross-antagonism. In addition, we tested a previously described alternative signaling pathway activated downstream of D_1R, Ca^{2+} mobilization (*Chen et al., 2007*; *Jose et al., 1995*). When cells were treated with the D_1R agonist SKF 81297 a robust and rapid increase in cytosolic Ca^{2+} was detected in both STHdh^{Q7} and STHdh^{Q111} cells (*Figure 1B,C*). Importantly, this calcium release could be dampened with the H_3R antagonist thioperamide (cross-antagonism) (*Figure 1B,C*). The above signaling data strongly support the presence of functional D_1R-H_3R heteromers in STHdh cells.

To further demonstrate that an H_3R antagonist is dampening D_1R activation involving D_1R-H_3R heteromers, we evaluated the effect of interfering peptides, which are synthetic peptides with the amino acid sequence of domains of the receptors involved in the heteromeric interface. This approach has been used by us and others to disrupt other heteromer complexes (*Bonaventura et al., 2015*; *Guitart et al., 2014*; *Hasbi et al., 2014*; *Lee et al., 2014*; *Viñals et al., 2015*). In a previous study we showed the efficacy of this approach in demonstrating heteromerization of D_1R with D_3R, using a peptide with the sequence of D_1R transmembrane domain 5 (TM5) but not TM7 (*Guitart et al., 2014*). We therefore investigated whether synthetic peptides with the sequence of TM5, and TM7 (as a negative control) of D_1R, fused to HIV-TAT, were also able to disrupt receptor D_1R-H_3R heteromers measured by PLA. In agreement with our hypothesis, there was a near complete loss in PLA fluorescence signal when STHdh^{Q7} and STHdh^{Q111} cells were incubated with TAT-TM five peptide (*Figure 1D,F*), but not for the negative control in which the TAT-TM seven peptide was used (*Figure 1H,J*). We next evaluated whether TM5 or TM7 would interfere with the observed cross-antagonism in calcium mobilization assays. Clearly, pretreatment of both STHdh^{Q7} and STHdh^{Q111} cells with the TAT-TM5 (*Figure 1E,G*) but not TAT-TM7 (*Figure 1I,K*) peptide disrupts the ability of the H_3R antagonist thioperamide to dampen D_1R calcium signaling. These results support that TM5 forms part of the interface of the D_1R-H_3R heteromer and demonstrate that the H_3R antagonist effect is driven through direct interaction between D_1R and H_3R.

H_3R ligands prevent the D_1R-induced cell death in STHdh^{Q7} and STHd^{Q111} cells

It has been previously reported that upon activation of D_1R, STHdh cell viability is reduced (*Paoletti et al., 2008*). To explore whether H_3R ligands could impair D_1R activation through D_1R-H_3R heteromers in a pathologically relevant readout, we used D_1R-induced cell death as an output of D_1R activation in STHdh cells. As expected, STHdh cell viability decreased when treated with the D_1R agonist SKF 81297 in a concentration-dependent manner (*Figure 1—figure supplement 2C*). Significant cell death did not occur until 30 μM SKF 81297 was used (*Figure 1—figure supplement 2C*), an effect prevented by the D_1R antagonist SCH 23390 (*Figure 1—figure supplement 2E*). Pretreatment with the H_3R antagonist thioperamide, which did not modify cell viability when administered alone (*Figure 1—figure supplement 2E*), increased the number of surviving cells in the presence of the D_1R agonist SKF 81297 in both cell types (*Figure 1L,M* and *Figure 1—figure supplement 2D*). Importantly, the effect of the H_3R antagonist thioperamide was specific since no protection from D_1R agonist-induced cell death was observed in cells depleted of H_3R with shRNA lentiviral infection (*Figure 1L,M*), but was observed in cells transfected with the control lentivirus (*Figure 1—figure supplement 2F*). In addition, we also demonstrated that recovery of viability induced by the H_3R antagonist thioperamide was mediated by D_1R-H_3R heteromers since pre-incubation with D_1R TM5 peptide, but not D_1R TM7 impaired the H_3R antagonist protection from D_1R agonist-induced cell death (*Figure 1L,M*).
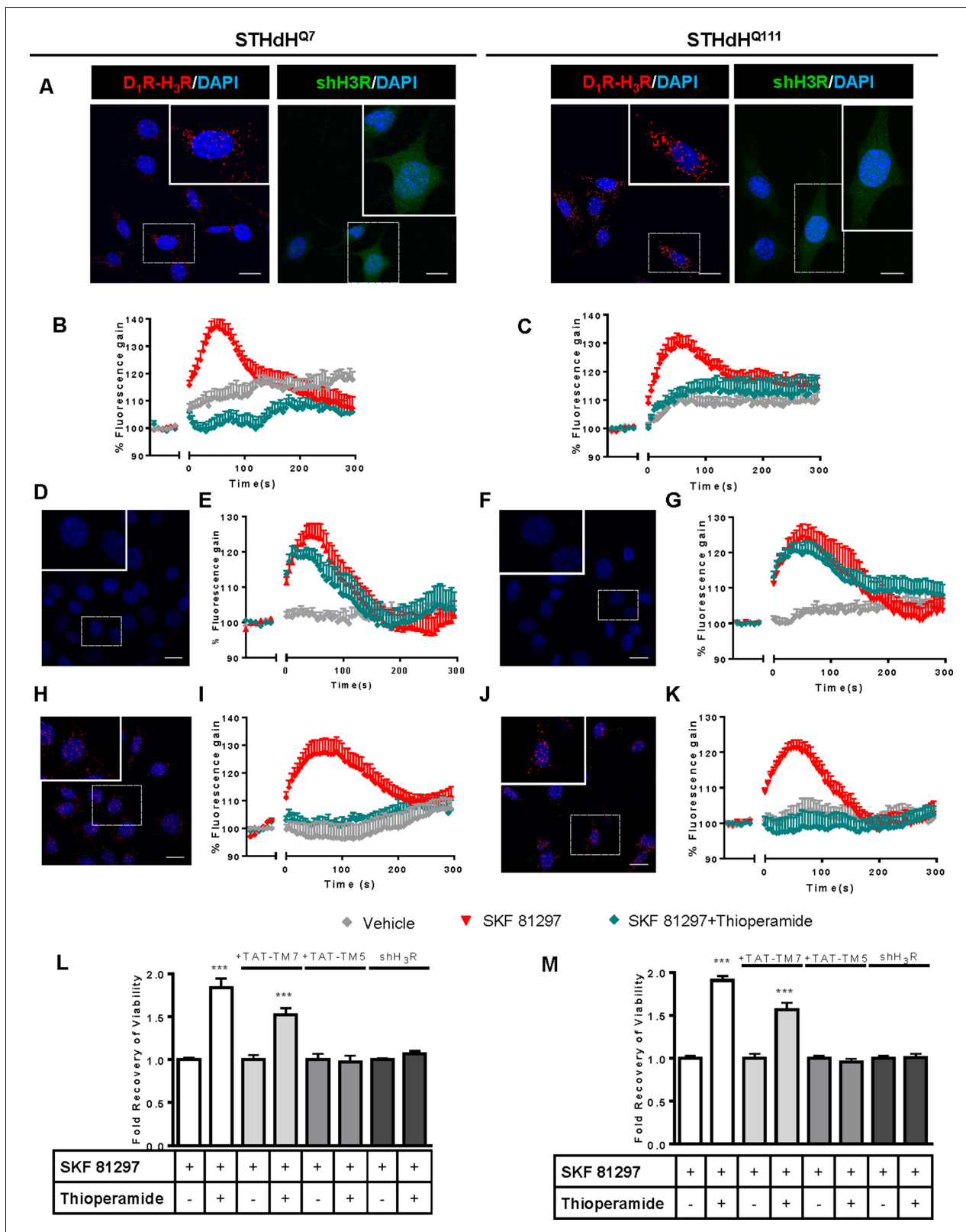
Figure 1. Functional D_1R-H_3R heteromers are expressed in $STHdh^{Q7}$ and $STHdh^{Q111}$ cells. PLA were performed in $STHdh^{Q7}$ and $STHdh^{Q111}$ cells (**A, D, F, H and J**) or in cells infected with shH_3R to silence H_3R, observed as green stained cells due to the GFP expression included in the plasmid (**A**). D_1R-H_3R heteromers were visualized in STHdh cells as red spots around blue colored DAPI stained nucleus, but not in STHdh cells infected with shH_3R vector (**A**). Calcium increases were measured in $STHdh^{Q7}$ (**B, E and I**) or $STHdh^{Q111}$ (**C, G and K**). Cells were treated (20 min) or not with the H_3R

Figure 1 continued on next page

Figure 1 continued

antagonist thioperamide (10 µM) before the addition of vehicle or SKF 81297 (1 µM). In (D, E, F, G, H, I, J and K), STHdH^{Q7} (D, E, H and I) or STHdH^{Q111} (F, G, J and K) cells were also pre-treated for 60 min with 4 µM TM5 (D, E, F and G) or TM7 (H, I, J and K) peptides. Heteromers were visualized as red spots around DAPI (blue) stained nucleus in cells pre-treated with TM7 peptide. Scale: 20 µm. For each calcium curve values are expressed as a percentage increase with respect to untreated cells and are a mean ± SEM of 3 to 5 independent experiments. In (L and M), cell viability was determined in STHdh^{Q7} (L) or STHdh^{Q111} cells (M) pre-treated for 60 min with vehicle (white columns), with 4 µM TAT-TM7 (pale grey columns) or TAT-TM5 (grey columns) or infected with shH$_3$R to silence H$_3$R (dark grey columns) prior overstimulation with 30 µM SKF 81297. Values represent mean ± SEM (n = 24 to 30) of cell viability recovery expressed as in-fold respect to SKF 81297 treated cells. Student's *t* test showed a significant (***p<0.001) effect over SKF 81297 treated cells.

The online version of this article includes the following figure supplement(s) for figure 1:

Figure supplement 1. Negative controls for Proximity Ligation Assays (PLA) in striatal cells not depleted or H$_3$R depleted by shRNA.

Figure supplement 2. H$_3$R ligands revert the D$_1$R-mediated decreases in STHdh^{Q7} and STHdh^{Q111} cell viability.

Figure supplement 3. Effect of low and high SKF 81297 concentrations in p-p38 and intracellular calcium release.

Figure supplement 4. H$_3$R ligands revert the D$_1$R-mediated decreases in cell viability in STHdh^{Q7} and STHdh^{Q111} by modulating calcium signaling and p38 phosphorylation.

Figure supplement 5. H$_3$R ligands revert the D$_1$R overstimulation-induced heteromer disruption in striatal cells.

To better understand the mechanisms involved in D$_1$R-H$_3$R heteromer action, we determined which cellular signaling pathways are implicated in the cross-antagonism of H$_3$R upon activation of D$_1$R. Both concentrations of the D$_1$R agonist SKF 81297, cytotoxic (30 µM) and non-cytotoxic (1 µM), can induce intracellular calcium release, which is more pronounced and persistent at 30 µM (*Figure 1—figure supplement 3A,B*). A correlation between the intensity of calcium responses and the activation of apoptotic pathways such as p38 (*Semenova et al., 2007*) has been previously demonstrated. Thus, we measured changes in p38 phosphorylation levels using both concentrations of the D$_1$R agonist SKF 81297 (*Figure 1—figure supplement 3C,D*). Interestingly, we found that increased phosphorylation of p38 only occurred at the cytotoxic concentration of SKF 81297. Similar to treatment with 1 µM SKF 81297 (see *Figure 1*), the calcium release induced by 30 µM SKF 81297 was also blocked by the H$_3$R antagonist thioperamide (*Figure 1—figure supplement 4A,B*). Treatment with the H$_3$R antagonist thioperamide reduced p38 phosphorylation upon D$_1$R activation in both cell types (*Figure 1—figure supplement 4C*). Moreover, the p38 inhibitor SB 203580 blocked p38 phosphorylation (*Figure 1—figure supplement 4C*) and protected against the cytotoxic effect of the D$_1$R agonist SKF 81297 in a dose-dependent manner (*Figure 1—figure supplement 4D*), confirming that p38 is a key pathway involved in D$_1$R-mediated cell death in these cells.

It has been reported that ligands can influence receptor oligomerization. To understand how the ligands used here might impact D$_1$R-H$_3$R heteromers we performed PLA after treating with either vehicle, SKF 81297 or SKF 81297 and thioperamide. We found that SKF 81297-induced a loss of PLA staining in both STHdh cells (*Figure 1—figure supplement 5*), while pre-treatment with the H$_3$R antagonist thioperamide preserved the number of punctate PLA spots (*Figure 1—figure supplement 5*).

Functional D$_1$R-H$_3$R heteromers are expressed in wild-type Hdh$^{Q7/Q7}$ and in Hdh$^{Q7/Q111}$ mutant knock-in mice at early but not late HD stages

To test whether D$_1$R-H$_3$R heteromers can indeed be targets for treating HD, we investigated their expression and function in the striatum, cerebral cortex and hippocampus of a widely accepted preclinical model of HD, the heterozygous Hdh$^{Q7/Q111}$ mutant knock-in mice, and their wild-type Hdh$^{Q7/Q7}$ littermates (*Giralt et al., 2012*; *Puigdellívol et al., 2015*). By PLA we confirmed that both Hdh$^{Q7/Q7}$ and Hdh$^{Q7/Q111}$ mice display D$_1$R-H$_3$R heteromers at 2 months (mo) (*Figure 2—figure supplement 1*) and four mo (*Figure 2A,B*) of age in all brain regions tested. No signal was observed in negative controls in which one of the PLA primary antibodies were missing (*Figure 2—figure supplement 2*). Heteromer expression was similar in all brain areas and no differences were observed between genotypes at 4 mo of age (*Figure 2B*). Surprisingly, an almost complete loss of D$_1$R-H$_3$R heteromers was found in 6 mo and eight mo-old Hdh$^{Q7/Q111}$ mice but not in Hdh$^{Q7/Q7}$ mice
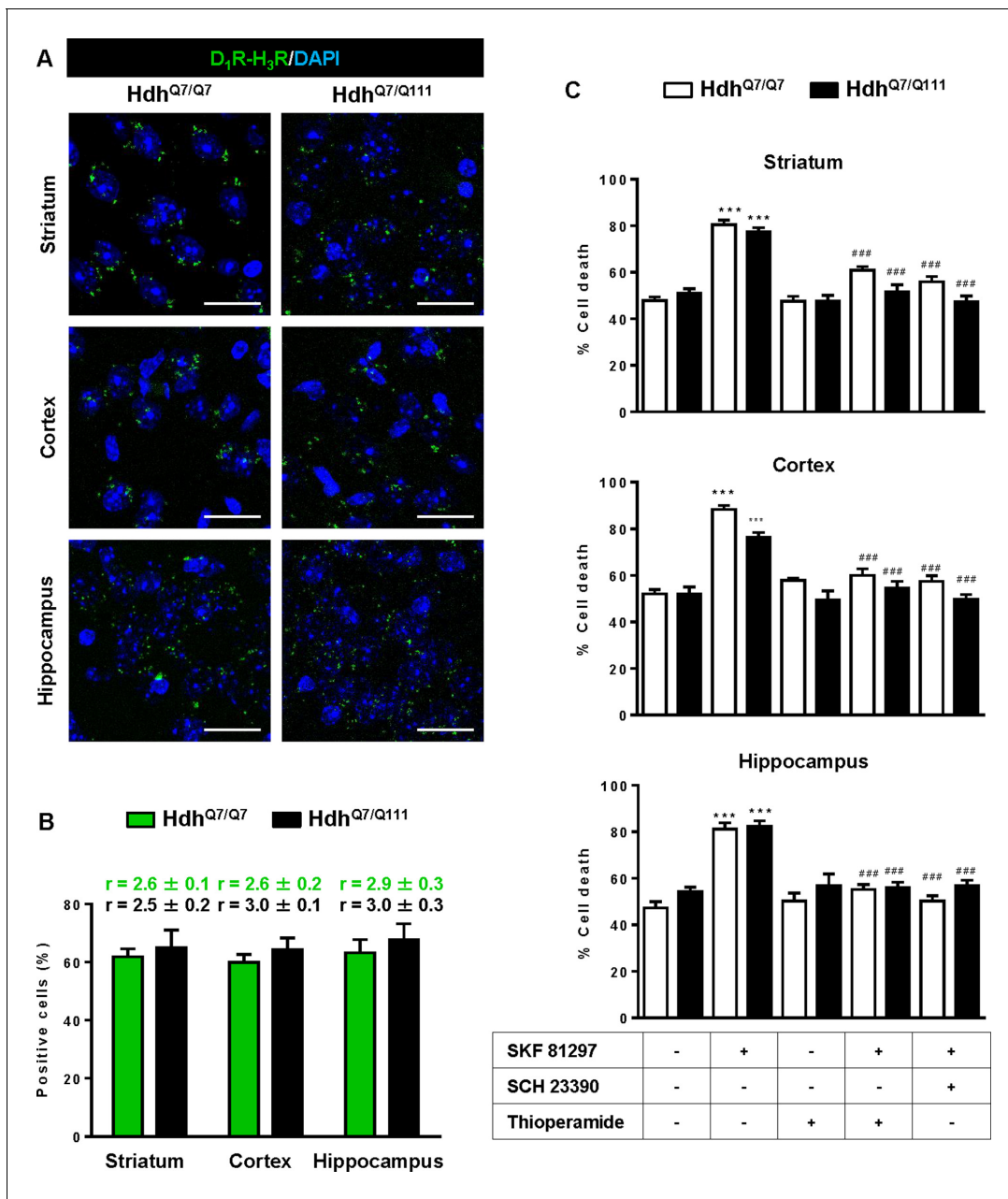
Figure 2. Functional D_1R-H_3R heteromers are expressed in wild-type $Hdh^{Q7/Q7}$ and mutant $Hdh^{Q7/Q111}$ mice. Striatal, cortical or hippocampal slices from 4-month-old $Hdh^{Q7/Q7}$ and $Hdh^{Q7/Q111}$ mice were used. In (A), by Proximity Ligation Assays (PLA) D_1R-H_3R heteromers were visualized in all slices as green spots around blue colored DAPI stained nucleus. Scale bar: 20 μm. In (B), the number of cells containing one or more green spots is expressed as the percentage of the total number of cells (blue nucleus). *r values* (number of green spots/cell containing spots) are shown above each bar. Data (% of positive cells or r) are the mean ± SEM of counts in 600–800 cells from 4 to 8 different fields from three different animals. Student's *t* test showed no significant differences in heteromers expression in $Hdh^{Q7/Q7}$ and $Hdh^{Q7/Q111}$ mice. In (C), striatal, cortical or hippocampal organotypic slice cultures from 4-month-old $Hdh^{Q7/Q7}$ and $Hdh^{Q7/Q111}$ mice were treated for 60 min with vehicle, the D_1R antagonist SCH 23390 (10 μM) or H_3R antagonist thioperamide (10 μM) before the addition of SKF 81297 (50 μM). After 48 h cell death was determined. Values represent mean ± SEM (n = 3 to 19) of percentage of cell death. One-way ANOVA followed by Bonferroni *post hoc* tests showed a significant effect over non-treated organotypic cultures (***p<0.001) or of the H_3R antagonist plus SKF 81297 treatment over the SKF 81297 (###p<0.001).

The online version of this article includes the following figure supplement(s) for figure 2:

Figure supplement 1. D_1R-H_3R heteromer are expressed in 2-month-old $Hdh^{Q7/Q7}$ and $Hdh^{Q7/Q111}$ mice.

Figure supplement 2. Negative controls for Proximity Ligation Assays (PLA) in mouse brain slices.

(*Figure 3—figure supplement 1* and *Figure 3A,B*), indicating that at more advanced disease stages the D_1R-H_3R heteromer is lost. Although at 8 mo of age we detected a partial decrease in striatal D_1R expression in Hdh$^{Q7/Q111}$ compared with Hdh$^{Q7/Q7}$ mice using ligand binding experiments (*Supplementary file 2*), the loss of heteromer expression is not due to a complete loss of receptor expression since by radioligand binding (*Supplementary file 2*) and mRNA expression analysis (*Supplementary file 3*) both receptors continue to be expressed.

To test the role of D_1R-H_3R heteromers, organotypic mouse striatal, cortical and hippocampal cultures were obtained. Cell death was induced by the D_1R agonist SKF 81297 (50 μM), and analysis of DAPI and propidium iodide staining was performed. As expected, D_1R agonist SKF 81297 treatment increased the percentage of cell death in all three regions compared to vehicle-treated organotypic cultures without significant differences between genotypes at 4 mo of age (*Figure 2C*). Importantly, slices pre-treated with the H_3R antagonist thioperamide, that does not modify cell death when administered alone, protected cells from D_1R elicited cell death in an equivalent manner to the D_1R antagonist SCH 23390 (*Figure 2C*), indicating that functional D_1R-H_3R heteromers are expressed in different brain areas of Hdh$^{Q7/Q7}$ and Hdh$^{Q7/Q111}$ mice at early disease stages. The dramatic change in heteromer expression in eight mo-old Hdh$^{Q7/Q111}$ mice was mirrored by the lack of protection of the H_3R antagonist thioperamide against SKF 81297-induced cell death in organotypic cultures (*Figure 3C*), corroborating that the presence of D_1R-H_3R heteromers is needed for the H_3R antagonist to prevent D_1R-mediated cell death.

Treatment with thioperamide prevents cognitive and motor learning deficits at early disease stages

To test whether the H_3R antagonist thioperamide can exert beneficial effects in the initial stages of the disease we evaluated the effect of chronic thioperamide treatment on motor learning and memory deficits in mutant Hdh$^{Q7/Q111}$ mice. Since cognitive decline is observed in these HD mice from 6 mo of age (*Brito et al., 2014*; *Giralt et al., 2012*; *Puigdellívol et al., 2015*) and the D_1R-H_3R heteromers are expressed and functional until the age of 5 mo (*Figure 4—figure supplement 1A,B*), we chose 5mo-old animals to start the thioperamide treatment (*Figure 4—figure supplement 2*). Corticostriatal function in saline and thioperamide-treated Hdh$^{Q7/Q7}$ and Hdh$^{Q7/Q111}$ mice was analyzed by using the accelerating rotarod task that evaluates the acquisition of new motor skills (*Puigdellívol et al., 2015*). Saline-treated mutant Hdh$^{Q7/Q111}$ mice were unable to maintain their balance on the rotarod as wild-type Hdh$^{Q7/Q7}$ mice revealing impaired acquisition of new motor skills (*Figure 4A*). Chronic treatment with thioperamide completely rescued motor learning deficits in mutant Hdh$^{Q7/Q111}$ mice as evidenced by a similar latency to fall in the accelerating rotarod as wild-type Hdh$^{Q7/Q7}$ mice. Next, recognition long-term memory (LTM) was analyzed by using the novel object recognition test (NORT) (*Figure 4B*). After two days of habituation in the open field arena (*Figure 4—figure supplement 3*), no significant differences were found between genotypes and/or treatments, demonstrating no alterations in motivation, anxiety or spontaneous locomotor activity. After habituation, animals were subjected to a training session in the open field arena in the presence of two similar objects (A and A'). Both saline and thioperamide-treated wild-type Hdh$^{Q7/Q7}$ and mutant Hdh$^{Q7/Q111}$ mice similarly explored both objects indicating neither object nor place preferences (*Figure 4B*). After 24 hr, LTM was evaluated by changing one of the old objects (A') for a novel one (B). Whereas saline-treated Hdh$^{Q7/Q111}$ mice did not show any preference for the novel object with respect to the familiar one, indicating recognition LTM deficits, thioperamide treatment completely prevented this LTM deficit in mutant Hdh$^{Q7/Q111}$ mice (*Figure 4B*). Next, spatial LTM was analyzed using the T-maze spontaneous alternation task (T-SAT) (*Figure 4C*). During the training, similar exploration time (*Figure 4C*, left panel) and similar number of arm entries (*Figure 4—figure supplement 4*, *left panel*) were found in all genotypes and treatments. After 5 hr, a testing session showed that saline-treated Hdh$^{Q7/Q111}$ mice had no preferences between the novel arm and the old arm, indicating spatial LTM deficits (*Figure 4C*, right panel). Interestingly, mutant Hdh$^{Q7/Q111}$ mice treated with thioperamide spent more time in the novel *versus* the old arm, revealing preserved LTM (*Figure 4C*, right panel). Overall, these data demonstrate the effectiveness of thioperamide treatment in restoring motor learning and preventing spatial and recognition LTM deficits in mutant Hdh$^{Q7/Q111}$ mice.

We next tested if the reversion of the HD phenotype in mutant Hdh$^{Q7/Q111}$ mice induced by thioperamide treatment correlated with the preservation of D_1R-H_3R heteromer expression. By PLA we
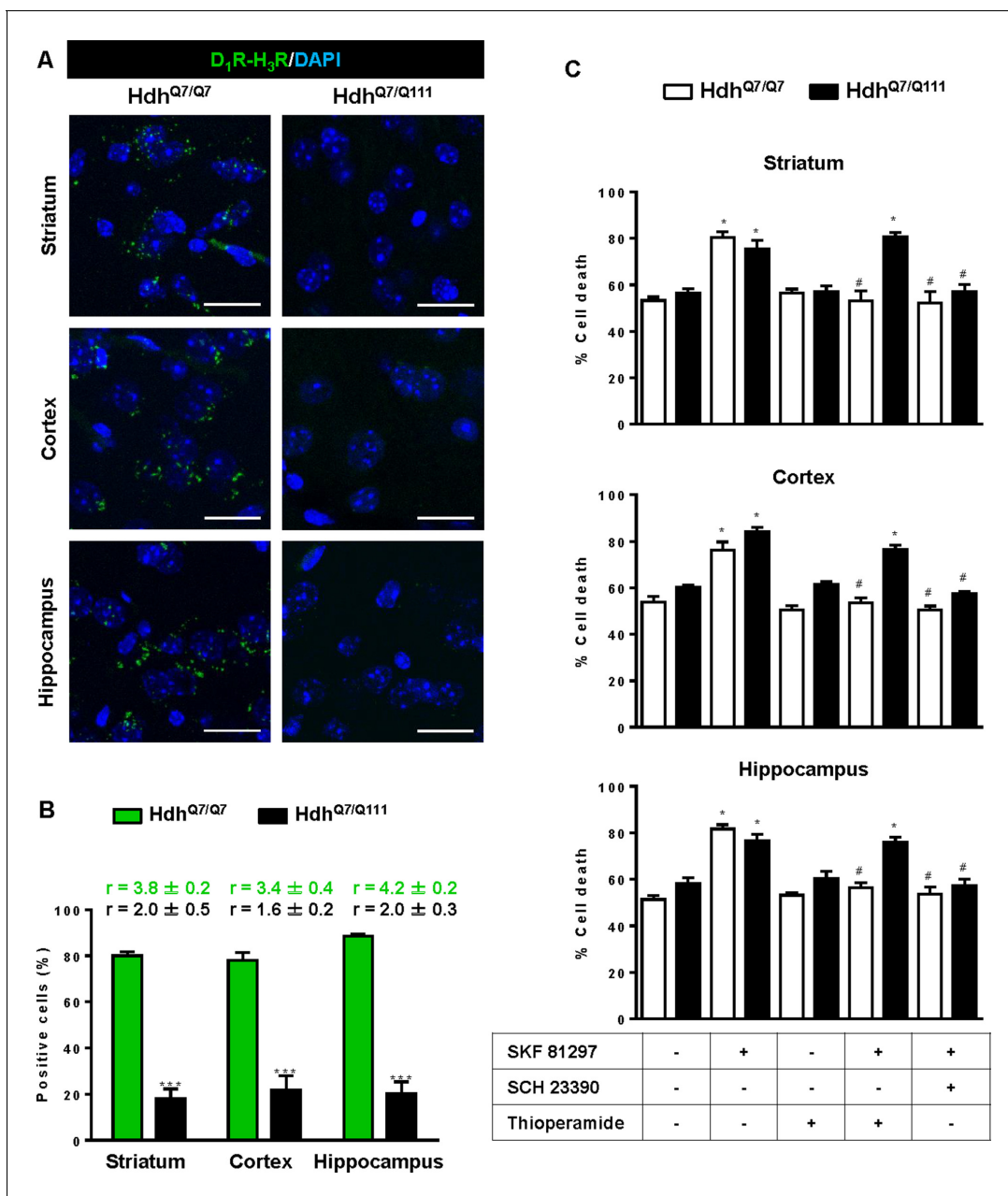
Figure 3. Functional D_1R-H_3R heteromers are expressed in wild-type $Hdh^{Q7/Q7}$ but not in 8-month-old mutant $Hdh^{Q7/Q111}$ mice. Striatal, cortical or hippocampal slices from 8-month-old $Hdh^{Q7/Q7}$ and $Hdh^{Q7/Q111}$ mice were used. In (**A**), by Proximity Ligation Assays (PLA) D_1R-H_3R heteromers were visualized in $Hdh^{Q7/Q7}$ mice but not in $Hdh^{Q7/Q111}$ mice as green spots around blue colored DAPI stained nucleus. Scale bar: 20 μm. In (**B**), the number of cells containing one or more green spots is expressed as the percentage of the total number of cells (blue nucleus). *r values* (number of green spots/cell containing spots) are shown above each bar. Data (% of positive cells or r) are the mean ± SEM of counts in 600–800 cells from 5 to 7 different fields from three different animals. Student's *t* test showed a significant (***$p < 0.05$) decrease of heteromers expression in $Hdh^{Q7/Q111}$ mice compared to the respective $Hdh^{Q7/Q7}$ mice. In (**C**) striatal, cortical or hippocampal organotypic slice cultures from 8-month-old $Hdh^{Q7/Q7}$ and $Hdh^{Q7/Q111}$ mice were treated for 60 min with medium, the D_1R antagonist SCH 23390 (10 μM) or the H_3R antagonist thioperamide (10 μM) before the addition of SKF 81297 (50 μM) and cell death was determined. Values represent mean ± SEM (n = 3 to 6) of percentage of cell death. One-way ANOVA followed by Bonferroni *post hoc* tests showed a significant effect over non-treated organotypic cultures (*$p < 0.05$) or of the H_3R antagonist plus SKF 81297 treatment over the SKF 81297 (#$p < 0.05$).

The online version of this article includes the following figure supplement(s) for figure 3:

Figure supplement 1. Expression of D_1R-H_3R heteromers in 6-month-old $Hdh^{Q7/Q7}$ and $Hdh^{Q7/Q111}$ mice chronically treated with saline.
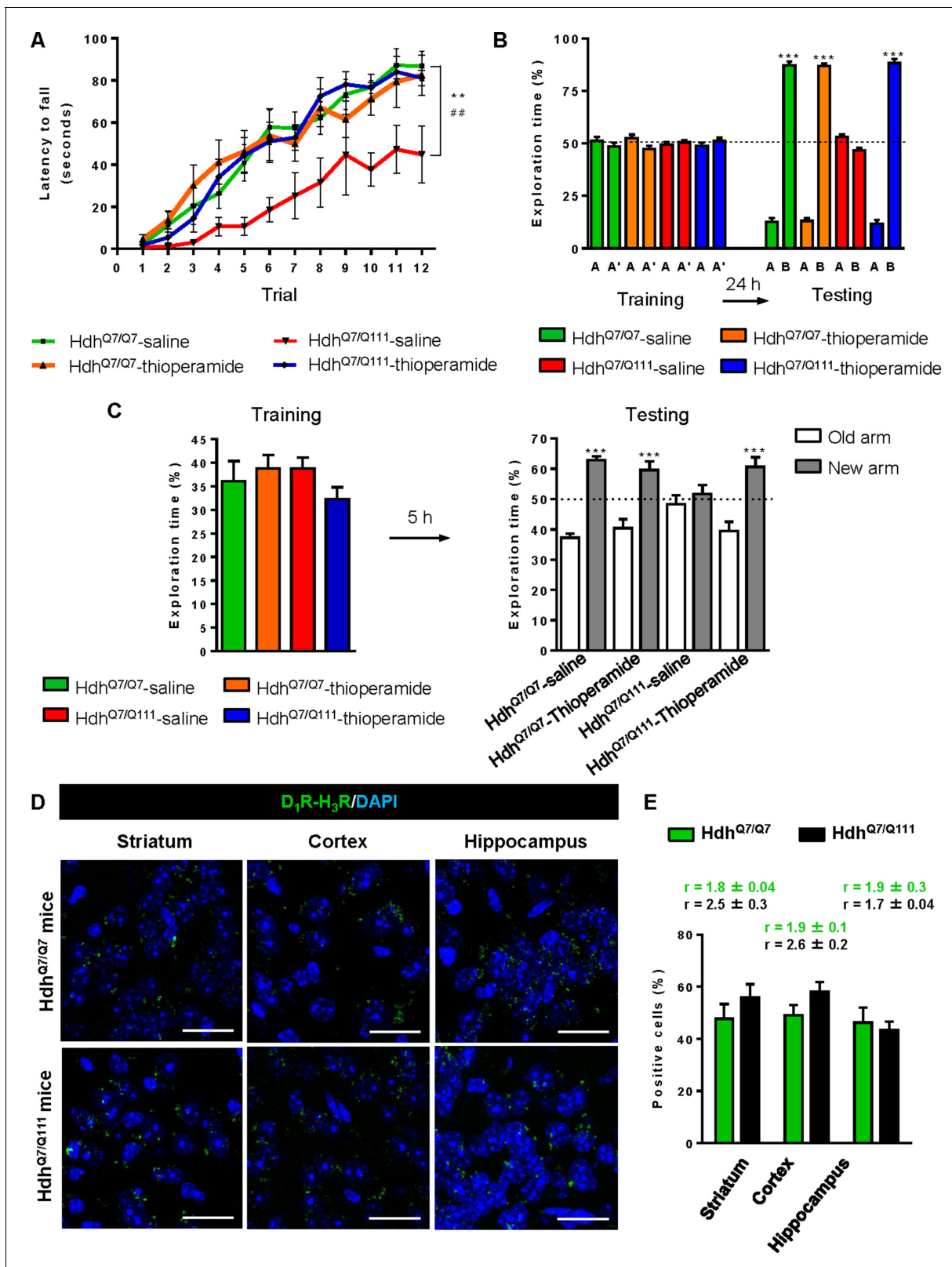
Figure 4. Thioperamide chronic treatment prevents motor learning, long-term memory (LTM) deficits and the loss of receptor heteromerization in 6-month-old Hdh^Q7/Q111 mice. In (**A**), curves illustrating the latency to fall in the accelerating rotarod of 6-month-old Hdh^Q7/Q7 and Hdh^Q7/Q111 mice treated with saline or thioperamide from 5 months of age are shown. In (**B**), the exploration time for saline or thioperamide-treated Hdh^Q7/Q7 and Hdh^Q7/Q111 mice during the training and the testing (24 hr delay, LTM) sessions in a novel-object recognition task showing that long-term recognition

Figure 4 continued on next page

Figure 4 continued

memory deficits are rescued in the thioperamide-treated Hdh$^{Q7/Q111}$ mice. One-way ANOVA with Bonferroni *post hoc* showed significant differences (***p<0.001) compared to the old object recognition. In (C), bar diagram illustrating the exploration time for saline- or thioperamide-treated Hdh$^{Q7/Q7}$ and Hdh$^{Q7/Q111}$ mice during the training and the 5 hr later testing in the T-SAT showing thioperamide reverses spatial long-term memory (LTM) deficits. In (A) to C), 11 saline-treated Hdh$^{Q7/Q7}$ mice, 10 thioperamide-treated Hdh$^{Q7/Q7}$ mice, seven saline-treated Hdh$^{Q7/Q111}$ mice and nine thioperamide-treated Hdh$^{Q7/Q111}$ mice were evaluated at 6 months of age. In (D) PLA were performed in striatal, cortical and hippocampal slices from 6-month-old Hdh$^{Q7/Q7}$ and Hdh$^{Q7/Q111}$ mice treated with thioperamide. D$_1$R-H$_3$R heteromers were visualized in all samples as green spots around blue colored DAPI stained nucleus. Scale bar: 20 μm. In (E) the right panel, the number of cells containing one or more green spots is expressed as the percentage of the total number of cells (blue nucleus). *r values* (number of green spots/cell containing spots) are shown above each bar. Data (% of positive cells or r) are the mean ± SEM of counts in 600–800 cells from 4 to 8 different fields from three different animals. Student's *t* test showed no significant differences in heteromer expression in thioperamide-treated Hdh$^{Q7/Q111}$ mice compared to the respective Hdh$^{Q7/Q7}$ mice.

The online version of this article includes the following figure supplement(s) for figure 4:

Figure supplement 1. Functional D$_1$R-H$_3$R heteromers are expressed in 5-month-old Hdh$^{Q7/Q7}$ and Hdh$^{Q7/Q111}$ mice.

Figure supplement 2. Schematic representation of pharmacological treatments and behavioral analysis performed after chronic treatment with saline or thioperamide.

Figure supplement 3. No significant differences in the open field habituation were found between treatments and genotypes.

Figure supplement 4. Training session in the T-SAT showed similar number of arm entries in all genotypes and treatments.

Figure supplement 5. Expression of D$_1$R-H$_3$R heteromers in 8-month-old Hdh$^{Q7/Q7}$ and Hdh$^{Q7/Q111}$ mice chronically treated with thioperamide.

observed that in saline-treated 6-mo-old Hdh$^{Q7/Q111}$ mice the heteromer expression was significantly diminished with respect to the age-matched Hdh$^{Q7/Q7}$ mice (*Figure 3—figure supplement 1A,B*). Notably, treatment with thioperamide significantly prevented the loss of D$_1$R-H$_3$R heteromers in all brain regions analyzed in Hdh$^{Q7/Q111}$ mice at both 6 (*Figure 4D,E*) and 8 mo of age (*Figure 4—figure supplement 5A,B*).

Treatment with thioperamide ameliorates spinophilin-immunoreactive puncta alterations in the motor cortex and hippocampus of 6-month-old mutant Hdh$^{Q7/Q111}$ mice

Alterations in dendritic spine dynamics, density and morphology are critically involved in the synaptic deficits present in HD (*Brito et al., 2014*; *Ferrante et al., 1991*; *Guidetti et al., 2001*; *Lynch et al., 2007*; *Milnerwood et al., 2006*; *Puigdellívol et al., 2015*; *Simmons et al., 2009*; *Sotrel et al., 1993*; *Spires et al., 2004*). We recently described a significant decrease in dendritic spine density in the hippocampus (*Brito et al., 2014*) and the motor cortex of mutant Hdh$^{Q7/Q111}$ mice (*Puigdellívol et al., 2015*) without significant alterations in the striatum. To analyze whether the improvement of motor learning and memory deficits observed in thioperamide-treated mutant Hdh$^{Q7/Q111}$ mice was associated with a recovery in the density of dendritic spines, spinophilin immunostaining was performed in CA1 hippocampal and motor cortical coronal slices obtained from 6-mo-old wild-type Hdh$^{Q7/Q7}$ and mutant Hdh$^{Q7/Q111}$ mice (*Figure 5A,B* and *Figure 5—figure supplement 1A*). This methodology was used by us and others to identify structural alterations in dendritic spines (*Hao et al., 2003*; *Puigdellívol et al., 2015*; *Tang et al., 2004*). Confocal microscopy analyses revealed a significant reduction in the density of spinophilin-immunoreactive puncta in the *stratum radiatum* (apical dendrites of CA1 pyramidal neurons) and *stratum oriens* (basal dendrites of CA1 pyramidal neurons) of saline-treated 6-mo-old mutant Hdh$^{Q7/Q111}$ mice compared to saline-treated wild-type Hdh$^{Q7/Q7}$ mice (*Figure 5A* and *Figure 5—figure supplement 1A*). Interestingly, thioperamide treatment prevented the decline in the number of spinophilin-immunoreactive puncta in mutant Hdh$^{Q7/Q111}$ mice (*Figure 5A* and *Figure 5—figure supplement 1A*). Similar data was obtained when the layers of the motor cerebral cortex (M1) were analyzed. A significant reduction in the density of spinophilin-immunoreactive puncta in layer I and layer II-III, but not layer V, of the motor cortex of 6-mo-old saline-treated Hdh$^{Q7/Q111}$ mice was found compared to saline-treated Hdh$^{Q7/Q7}$ mice (*Figure 5B* and *Figure 5—figure supplement 1A*). Interestingly, thioperamide-treated Hdh$^{Q7/Q111}$ mice exhibited a complete recovery in the density of spinophilin-immunoreactive puncta (*Figure 5B* and *Figure 5—figure supplement 1A*). No significant differences were found between groups when the mean size of spinophilin puncta was analyzed (*Figure 5—figure*
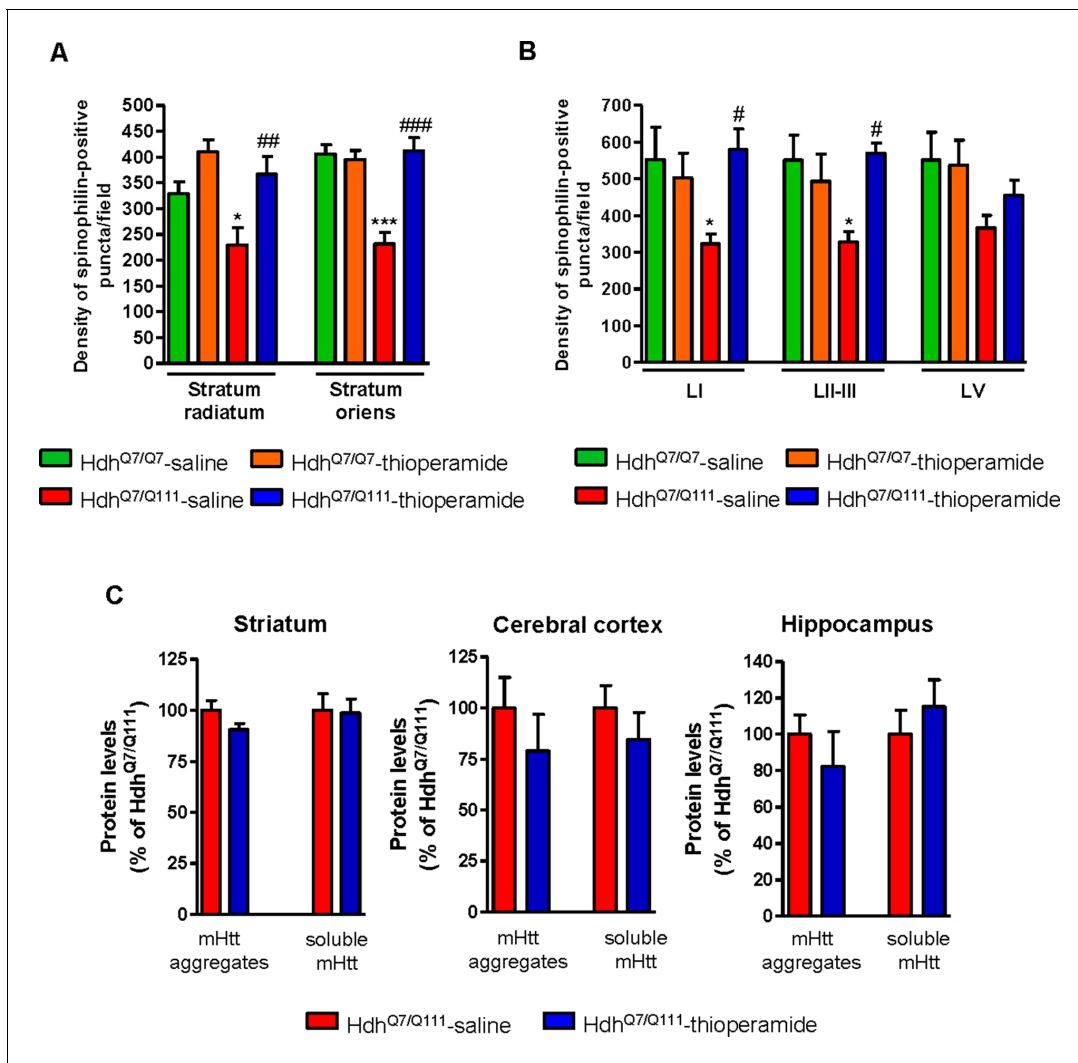
Figure 5. Thioperamide treatment restored spinophilin-immunoreactive puncta reduction in the hippocampus and motor cortex of Hdh$^{Q7/Q111}$ mice and exerts no effect on the clearance of mutant huntingtin accumulation. In (A) spinophilin-immunoreactive puncta were counted in the *stratum oriens* and *stratum radiatum* of CA1 hippocampus and in (B) layers I, II/III and V of motor cortex area 1 (M1) of saline and thioperamide-treated Hdh$^{Q7/Q7}$ and Hdh$^{Q7/Q111}$ mice. Quantitative analysis is shown as mean ± SEM (n = 9 images from three animals/group). Statistical analysis was performed using Student's two-tailed *t* test. *p<0.05, ***p<0.001 compared to saline-treated Hdh$^{Q7/Q7}$ mice. #p<0.05, ##p<0.01, ###p<0.001 compared to saline-treated Hdh$^{Q7/Q111}$ mice. In (C), Quantification of the protein levels of insoluble mHtt oligomeric forms and soluble mHtt forms of total striatal, hippocampal and cortical extracts from 6-month-old saline and thioperamide-treated Hdh$^{Q7/Q111}$ mice analysed by immunoblot. All histograms represent the mean ± SEM (n = 6–8 per group). Student's *t* test showed no significant differences between groups.

The online version of this article includes the following figure supplement(s) for figure 5:

Figure supplement 1. Biochemical and Pathological Effects of Thioperamide treatment.

supplement 1A). Altogether, these data demonstrate that the loss of spinophilin immunoreactive-puncta in mutant Hdh$^{Q7/Q111}$ mice can be ameliorated by thioperamide treatment.

We also evaluated mutant huntingtin (mhtt) aggregates in the striatum, cerebral cortex and hippocampus of mutant Hdh$^{Q7/Q111}$ mice after saline or thioperamide treatment, as another pathological hallmark of HD (*Arrasate and Finkbeiner, 2012*; *Giralt et al., 2012*; *Hoffner et al., 2007*). 1C2 immunostaining revealed in lysates from either vehicle or treated mutant Hdh$^{Q7/Q111}$ mice a substantial accumulation of mhtt oligomeric forms detected as a diffuse smear in the stacking gel (*Figure 5—figure supplement 1B*). Thioperamide treatment failed to prevent the accumulation of these

oligomeric forms (*Figure 5C* and *Figure 5—figure supplement 1B*). No significant differences between groups were found when soluble monomeric mhtt levels were analyzed (*Figure 5C* and *Figure 5—figure supplement 1B*).

Thioperamide treatment does not rescue memory and motor learning deficits in mutant Hdh$^{Q7/Q111}$ mice when D$_1$R-H$_3$R heteromers are lost

If the behavioral improvements observed after thioperamide treatment are mediated by the D$_1$R-H$_3$R heteromer and not just by the blockade of the single H$_3$R, then a treatment paradigm in the absence of the heteromer should have no effect. To test this hypothesis, we used wild-type Hdh$^{Q7/Q7}$ and mutant Hdh$^{Q7/Q111}$ mice at the age of 7 months, when we found the heteromer to be lost. Animals were chronically treated with saline or thioperamide for 1 month and motor learning was evaluated using the accelerating rotarod task. As expected, saline-Hdh$^{Q7/Q111}$ mice exhibited poor performance in this task showing shorter latency to fall compared to wild-type Hdh$^{Q7/Q7}$ mice (*Figure 6A*). Notably, thioperamide treatment had no effect on motor learning performance as both saline- and thioperamide-treated mutant Hdh$^{Q7/Q111}$ mice were indistinguishable demonstrated by similar latency to fall in the accelerating rotarod task (*Figure 6A*).

We next asked whether thioperamide treatment could improve cognitive function by rescuing memory deficits in these same animals. Saline-treated 8-mo-old Hdh$^{Q7/Q111}$ mice exhibited long-term memory deficits when recognition memory was analyzed using the novel object recognition test (NORT) (*Figure 6B*). Similar to motor learning results, chronic treatment with thioperamide did not rescue Hdh$^{Q7/Q111}$ mice from memory deficits (*Figure 6B*). Overall, these results demonstrate that the effect of thioperamide in learning and memory in Hdh$^{Q7/Q111}$ mice requires the proper expression and function of D$_1$R-H$_3$R heteromers.

D$_1$R-H$_3$R heteromer expression changes occur in other rodent HD models and in HD patients

The fact that thioperamide treatment 1) prevents cognitive and motor learning deficits, 2) ameliorates striatal neuropathology, 3) ameliorates morphological alterations and 4) prevents the loss of D$_1$R-H$_3$R heteromers at 6 mo and 8 mo of age in a mouse model of HD is suggestive that thioperamide, or a future pharmacologically improved H$_3$R antagonist specifically targeting D$_1$R-H$_3$R heteromers, can be used to treat HD symptoms. To test this, we investigated D$_1$R-H$_3$R heteromer expression in other transgenic HD mouse models and in human caudate-putamen slices using PLA. The loss of heteromer expression compared with wild-type littermates was also observed in other mouse models of HD, the R6/1 and R6/2 mice transgenic for the human huntingtin exon 1 (*Figure 7—figure supplement 1A,B*, respectively). Importantly, D$_1$R-H$_3$R heteromers were detected as green spots surrounding the blue stained nuclei in human caudate-putamen slices from control individuals and low-grade (grade 0, 1 and 2) HD patients (*Figure 7A,B*). In contrast, green spots were almost absent in samples from high-grade (grade 3 or grade 4) HD patients (*Figure 7A,B*). These results show that D$_1$R-H$_3$R heteromer formation changes during disease progression and, importantly, that humans express D$_1$R-H$_3$R heteromers at early disease stages.

Discussion

The imbalance of dopamine inputs throughout HD progression represents a potential 'point of no return' for HD patients as this disequilibrium can eventually lead to substantial neuronal dysfunction and cell death. In the present study, we demonstrate that 1) excess dopamine signaling via D$_1$R leads to cell death by activating the p38 pathway; 2) D$_1$R-H$_3$R complexes are found within the striatum, cortex and hippocampus of WT mice and in HD mice at early but not late disease stages; 3) targeting D$_1$R via D$_1$R-H$_3$R complexes can slow progression of the disease in early but not late stages when the complexes are lost; and 4) D$_1$R-H$_3$R complexes are expressed in the human brain and thus represent potential therapeutic targets. This is the first demonstration of GPCR heteromers as potential targets to treat HD. Together, these data support a novel role for D$_1$R-H$_3$R complexes in neuroprotection and HD.

Several studies have revealed that dopamine neurotoxicity increases the sensitivity of MSSNs to glutamate inputs and leads to striatal neurodegeneration, a role ascribed to aberrant D$_1$R and not D$_2$R (*Cepeda and Levine, 1998*; *Flores-Hernández et al., 2002*; *Paoletti et al., 2008*; *Tang et al.,*
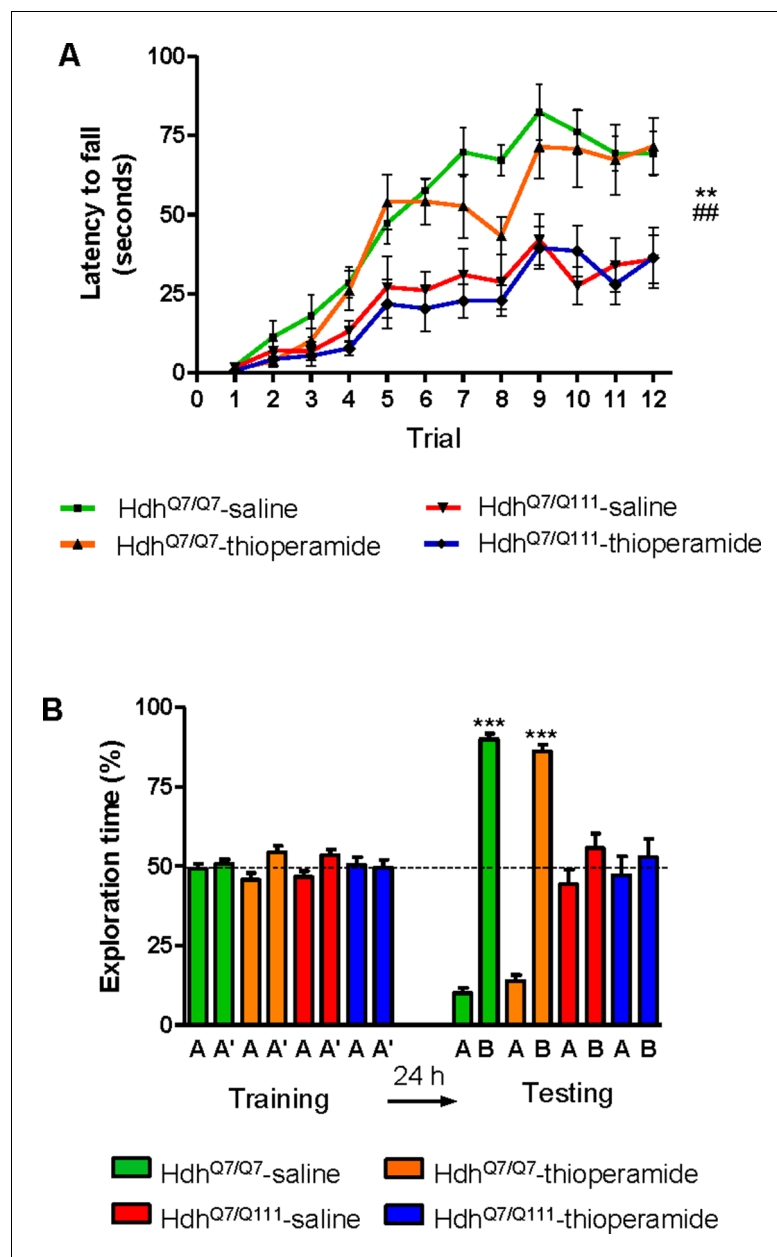
Figure 6. Thioperamide chronic treatment does not prevent motor learning and long-term memory (LTM) deficits in 8-month-old Hdh$^{Q7/Q111}$ mice when the D$_1$R-H$_3$R heteromer is not expressed. In (**A**), curves illustrating the latency to fall in the accelerating rotarod of 8-month-old Hdh$^{Q7/Q7}$ and Hdh$^{Q7/Q111}$ mice treated with saline or thioperamide from 7 months of age are shown. Two-way ANOVA with repeated measures showed significant differences (**$p<0.01$) of saline-treated Hdh$^{Q7/Q111}$ mice compared to saline-treated Hdh$^{Q7/Q7}$ mice or (##$p<0.01$) thioperamide-treated Hdh$^{Q7/Q111}$ mice compared to saline-treated Hdh$^{Q7/Q7}$ mice. 11 saline-treated Hdh$^{Q7/Q7}$ mice, 11 thioperamide-treated Hdh$^{Q7/Q7}$ mice, eight saline-treated Hdh$^{Q7/Q111}$ mice and nine thioperamide-treated Hdh$^{Q7/Q111}$ mice were evaluated at 8 months of age. In (**B**), bar diagram illustrating the exploration time for saline or thioperamide-treated Hdh$^{Q7/Q7}$ and Hdh$^{Q7/Q111}$ mice during the training and the testing (24 hr delay, LTM) sessions in a novel-object recognition task showing that long-term recognition memory deficits are not rescued in the thioperamide-treated Hdh$^{Q7/Q111}$ mice. One-way ANOVA with Bonferroni *post hoc* comparisons showed significant differences (***$p<0.001$) compared to the old object recognition. 11 saline-treated Hdh$^{Q7/Q7}$ mice, 12 thioperamide-treated Hdh$^{Q7/Q7}$ mice, 10 saline-treated Hdh$^{Q7/Q111}$ mice and 11 thioperamide-treated Hdh$^{Q7/Q111}$ mice were evaluated at 8 months of age.
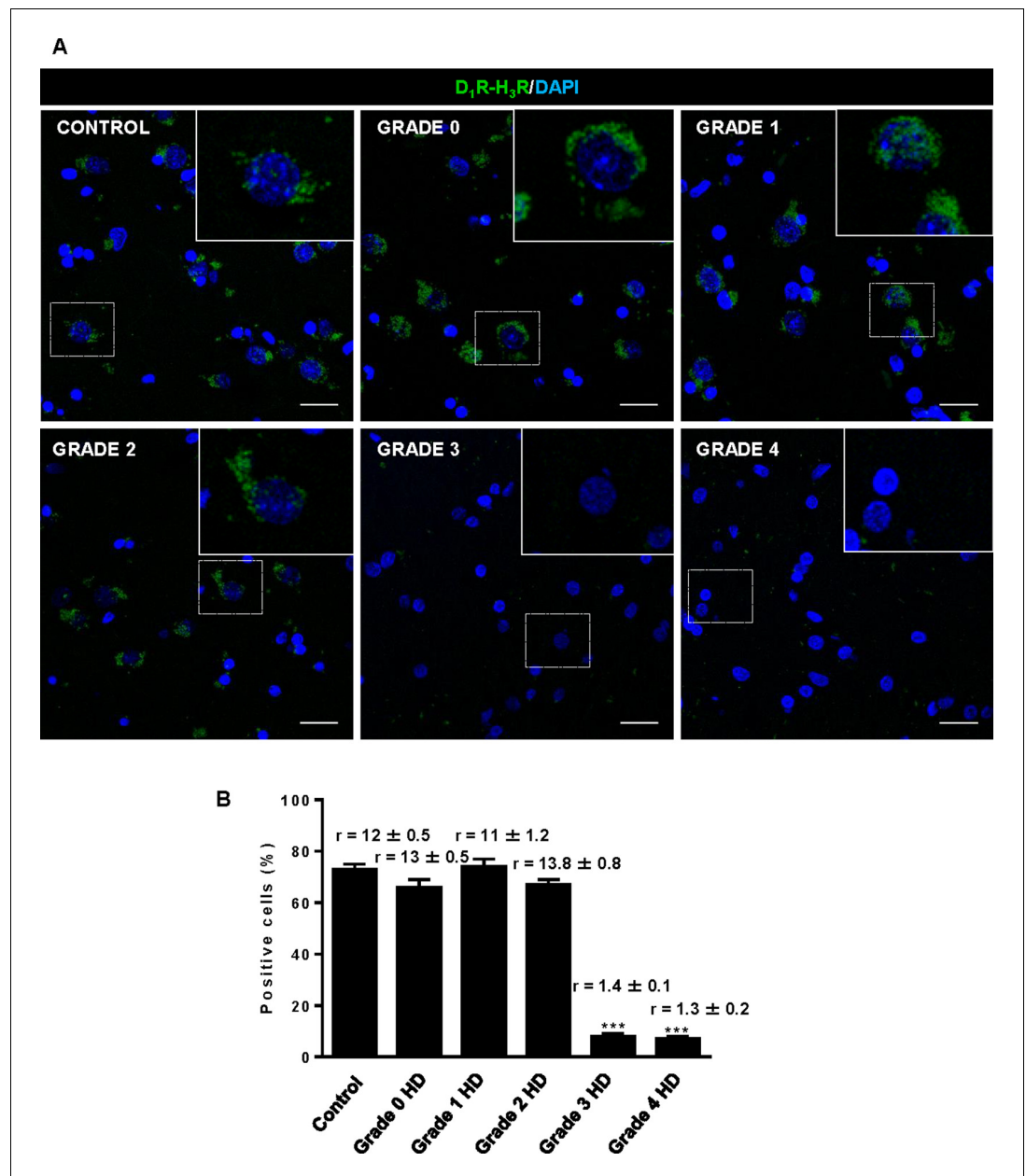
Figure 7. Striatal D_1R-H_3R heteromers are expressed in human control subjects and grade 2 HD patients but not in grade 3–4 HD patients. In (**A**), by Proximity Ligation Assays (PLA), D_1R-H_3R heteromers were visualized as green spots around blue colored DAPI stained nucleus in human striatal slices from age matched control subjects and 0–2 grade HD patients but not in 3–4 grade HD patients. Scale bar: 20 µm. In (**B**), the number of cells containing one or more green spots is expressed as the percentage of the total number of cells (blue nucleus). *r values* (number of green spots/cell containing spots) are shown above each bar. Data are mean ± SEM of counts in 600–800 cells from 10 different fields from subject described in Materials and Methods. Student's *t* test showed a significant (***p<0.001) decrease of heteromers expression in 3–4 grade HD patients compared to control subjects.

The online version of this article includes the following figure supplement(s) for figure 7:

Figure supplement 1. D_1R-H_3R heteromer are not expressed in HD R6/1 and R6/2 mouse models.

2007). Thus, pharmacological treatments aimed to reduce D_1R signaling may be beneficial to prevent or slow striatal cell death. Although we cannot rule out the participation of D_2R in striatal degeneration, our results suggest that D_1R is a major executor of the final signaling cascades that lead to cell death in HD. This is further supported by the fact that D_1R is in excess over D_2R in the striatum, so it is plausible that the former will be more significantly activated than the latter at increased DA levels. We have demonstrated that a toxic but not sub-toxic concentration of SKF81297 activates the p38 pro-apoptotic pathway, despite both concentrations triggering calcium release, albeit at different levels. Accordingly, p38 inhibitors completely abrogated the cell death induced by SKF81297 treatment, supporting the benefits of modulation of D_1R signaling as potential treatment in HD. However, direct manipulation of DA production and/or D_1R signalling via a specific antagonist has limited therapeutic ability due to associated deleterious side effects. An alternative approach is to modify D_1R signalling via the histamine neuromodulator. An interaction between H_3R and the dopaminergic system has been previously reported by us and others (*Kononoff Vanhanen et al., 2016*; *Rapanelli et al., 2016*; *Rapanelli et al., 2014*). In this frame, we have demonstrated that H_3R ligands completely abrogate striatal cell death induced by D_1R, likely by inhibition of D_1R-mediated calcium influx and p38 activation. Importantly, D_1R-H_3R complexes were found in the striatum, cortex and hippocampus from wild-type $Hdh^{Q7/Q7}$ and mutant $Hdh^{Q7/Q111}$ mice, regions known to be affected by mutant huntingtin toxicity (*Reiner et al., 1988*; *Rosas et al., 2003*; *Vonsattel and DiFiglia, 1998*).

The mechanisms of action of D_1R-H_3R heteromers can be multiple including allosteric effects. Indeed, the efficacy of the disrupting peptides supports protein-protein-driven effects. A second and potentially additional mechanism is that heteromer formation may alter the trafficking of D_1R, which could have pleiotropic consequences on signaling. For example it is known that overstimulation of D_1R induces receptor internalization promoting rapid intracellular signaling (*Kotowski et al., 2011*) and that receptor internalization can activate secondary signaling pathways (*Lohse and Calebiro, 2013*). We observe in vitro that thioperamide treatment maintains the PLA signal while in vivo we see similar effects. The signaling effects we observe appears to be on a variety of concentrations and timescales in agreement with previous studies showing that GPCR signaling occurs with varied kinetics (*Calebiro et al., 2010a*; *Calebiro et al., 2010b*). Indeed, part of the concern of trying to target GPCR heteromers for therapeutic purposes is the uncertainty around their stability and thus indirectly whether they can impact GPCR signaling at every timescale. For the case of D_1R-H_3R heteromers, it appears that they are stable enough that they can affect both rapid receptor signaling (e.g., Ca^{2+} mobilization) and longer cell signaling pathways like p38, two events that have previously been involved in neuronal cell death in HD (*Dau et al., 2014*; *Fan et al., 2012*; *Muller and Leavitt, 2014*; *Taylor et al., 2013*; *Wang et al., 2013*). It is unclear what controls D_1R-H_3R heteromer formation or why it is lost during progression of HD. Whether it is a change in expression of an accessory protein, a post-translational modification or a change in cell physiology/morphology remains to be explored.

Our findings do not rule out that H_3R ligands by targeting D_2R-H_3R heteromers (*Ferrada et al., 2008*) could block D_2R signaling and contribute to cell death protection. However, several findings argue in favor of D_1R-H_3R heteromer as uniquely responsible for the effects of thioperamide on cell death reduction. First, D_1R over-activation induces cell death-related pathways and D_1R-H_3R disruption. In addition, pre-treatment with H_3R ligands can block D_1R-induced cell death and prevent D_1R-H_3R loss. Finally, the effect of TAT-peptide analogues of D_1R transmembrane domains in D_1R-H_3R stability and function demonstrate that we are observing specific D_1R-H_3R, and not D_2R-H_3R, signaling and function. Thioperamide has recently been suggested to act via the H_4R receptor. However, several pieces of our data suggest H_4R is not responsible for the observed effects. First, we measured similar effects using VUF 5681, a different H_3R antagonist. In addition we lose all effects of thioperamide in cells where H_3R expression was silenced or when D_1R-H_3R heteromers are lost in the mice yet H_4R should still be expressed. Finally, H_4R is thought to be mainly expressed peripherally, while our data from brain slices and from mice which are predominatly cognitive in nature, strongly implicate the CNS.

Besides striatal and cortical cell death, growing evidence points to neuronal dysfunction as responsible for the earliest HD disturbances in cognitive and behavioral changes (*Lemiere et al., 2004*; *Puigdellívol et al., 2016*). Despite these early changes, no effective treatments are currently available to treat cognitive decline in HD. Moreover, the timing of intervention is also critical since

atrophy and dysfunction progress with age and treatment may be different according to the stage of illness. In this scenario, and given the well-known role of both dopamine and histamine in synaptic plasticity and memory (*Cahill et al., 2014*; *Ellender et al., 2011*; *Haas et al., 2008*; *Komater et al., 2005*; *López de Maturana and Sánchez-Pernaute, 2010*; *Mohsen et al., 2014*; *Orsetti et al., 2002*; *Pascoli et al., 2009*; *Wiescholleck and Manahan-Vaughan, 2014*), it is possible that the therapeutic potential of H_3R ligands as modulators of D_1R-H_3R heteromers could also be extended to improve learning impairments and cognitive decline in HD. This is supported by our data showing that chronic treatment with the H_3R antagonist thioperamide at 5 months of age prevented motor learning deficits, as well as impaired spatial and recognition memories in mutant $Hdh^{Q7/Q111}$ mice. Importantly, thioperamide treatment does not induce off-target effects (such as alterations in spontaneous locomotor activity or anxiety-like behaviors) neither in wild-type $Hdh^{Q7/Q7}$ nor in mutant $Hdh^{Q7/Q111}$ mice. In addition, early chronic treatment with thioperamide prevented disruption of the heteromer at 6 and 8 months of age and the subsequent cognitive decline. It seems unlikely that there is a direct link between D_1R-H_3R heteromers and cognitive deficits, but the data do suggest that whatever neuronal changes occur during progression of the disease they are blocked or at minimum delayed. Importantly, we can say that D_1R-H_3R heteromers are required for this effect as thioperamide treatment at 7 months of age (when the heteromer is lost in HD mice) is not able to prevent cognitive and motor learning deficits. This latter result might explain the results of the effects that GSK189254, an H_3R antagonist, have in a Q175 mouse model of HD (*Whittaker et al., 2017*). The authors saw no change in motor performance and mild improvement in exploratory behavior as measured in the Open Field test and in cognitive function as measured by a T-maze. Our data suggest that D_1R-H_3R heteromer expression is crucial to the efficacy of H_3R antagonists as a therapeutic option in HD.

What disease-driven neuronal changes are prevented by H_3R antagonism through the D_1R-H_3R heteromer is not completely clear. However, we did find that chronic thioperamide treatment at early stages completely rescue the reduction in the density of spinophilin-immunoreactive puncta in HD mice in both hippocampal and cortical areas, suggesting that adequate dopaminergic signaling is required for normal forms of synaptic structural plasticity and cognitive processes. Substantial data support the importance of dopamine receptors for synaptic plasticity in the cortex and hippocampus (*Levy and Goldman-Rakic, 2000*; *Robbins, 2000*; *Sajikumar and Frey, 2004*). In this view, any dopamine imbalance with both suboptimal and supra-optimal dopamine activity has been reported to modify cognitive performance (*Mattay et al., 2003*; *Vijayraghavan et al., 2007*). As the early stages of HD may reflect a hyperdopaminergic stage (*Chen et al., 2013a*; *Mochel et al., 2011*), treatments reducing dopamine signaling may have therapeutic benefits. In fact, dopamine-depleting drugs such as tetrabenazine or dopamine-stabilizers as pridopidine showed neuroprotective effects in HD mice (*Wang et al., 2010*), and improve motor coordination abnormalities in HD patients (*Huntington Study Group, 2006*; *de Yebenes et al., 2011*), while specific D_1R inhibition rescues electrophysiological changes in excitatory and inhibitory synaptic transmission in full-length HD mouse models (*André et al., 2011b*). However, none of these treatments have demonstrated cognitive improvements. The suggestion that D_1R-H_3R heteromers may be legitimate targets for the treatment of HD shines a spotlight on what continues to be an elusive drug target. Indeed, in the context of this study, the loss of the heteromer in disease progression despite the fact that the receptors themselves are still expressed and functional, points to the heteromers as optimal targets rather than the single receptors. The concept of heteromers have been known for over a decade but physiologic examples have only recently come to be appreciated (*Bonaventura et al., 2015*; *Viñals et al., 2015*; *Baba et al., 2013*; *Fribourg et al., 2011*; *González et al., 2012a* *González et al., 2012b*; *Kern et al., 2012*; *Navarro et al., 2015*). In sum, our study showing that H_3R antagonists can prevent learning and memory deficits by blocking D_1R in D_1R-H_3R complexes, along with the role of these heteromers on neuronal cell death, predict a critical role of the histaminergic system as modulator of the dopamine imbalance in HD, and may help to overcome the deleterious effects of directly manipulating DA-production and/or signaling, thus opening new and important alternatives for HD therapeutics.

Materials and methods

Key resources table

Reagent type (species) or resource	Designation	Source or reference	Identifiers	Additional information
Cell line (*H. sapiens*)	HEK293 (Human embryonic kidney293 cells)	American Type Culture Collection		
Cell line (*M. musculus*)	STHdh^{Q7}; STHdh^{Q111} (mouse striatal neuronal progenitor cells)	Dr M Macdonald (Center for Genomic Medicine, Boston, USA)		
Strain, strain background (*Mus musculus*)	Hdh$^{Q7/Q111}$; Hdh$^{Q7/Q7}$	Dr M Macdonald (Center for Genomic Medicine, Boston, USA)	Hdh^{Q111} MGI:1861935	
Strain, strain background (*Mus musculus*)	R6/1; R6/2	The Jackson Laboratory (Bar Harbor, ME, USA)	R6/1: MGI:2389466 For R6/2: MGI:2386951	
Strain, strain background (*H. sapiens*)	*Post-mortem* human brain sections containing caudate-putamen	Tissue Bank at Hospital Universitario Fundación Alcorcón (Madrid, Spain) Netherlands Brain Bank (Amsterdam, The Netherlands)		For details and characteristics of human samples see: "Moreno E., et al., Neuropsychopharmacology. 2018 PMID:28102227'
Antibody	anti-D$_1$R (guinea pig)	Frontier Institute	Cat. # D-1R-GP-Af500 RRID:AB_2571595	Dilution: 1/200; 1/100
Antibody	anti-H$_3$R (rabbit polyclonal)	Alpha diagnostic	Cat. # H3R31-A RRID:AB_1617140	Dilution: 1/200
Antibody	goat Alexa Fluor 488 anti-guinea pig antibody	Jackson Immunoresearch Laboratories	Cat. #106-545-003 RRID:AB_2337438	Dilution: 1/100
Antibody	anti-phospho-p38 MAPK (Thr180/Tyr182) (rabbit polyclonal)	Cell Signaling	Cat. #9211S RRID:AB_331641	Dilution: 1/1,000
Antibody	anti-β-tubulin (mouse monoclonal)	Sigma	Cat# SAB4200715 RRID:AB_2827403	Dilution: 1/10,000
Antibody	IRDye 680 goat anti-rabbit antibody	Li-cor	Cat. #926–68071 RRID:AB_10956166	Dilution: 1/10,000
Antibody	IRDye 800 goat anti-mouse antibody	Li-cor	Cat. # 926–32210 RRID:AB_621842	Dilution: 1/10,000
Antibody	anti-spinophilin (rabbit polyclonal)	Millipore	Cat# 06–852 RRID:AB_310266	Dilution: 1/250
Antibody	Cy3 anti-rabbit secondary antibodies	Jackson Immuno Research Laboratories	Cat# 111-165-003 RRID:AB_2338000	Dilution: 1/200
Antibody	Anti-1C2 (mouse monoclonal)	Millipore	Cat# MAB1574 RRID:AB_94263	Dilution: 1/1,000
Recombinant DNA reagent	Clone V3LHS_638095	Thermo Scientific		
Recombinant DNA reagent	Clone V3LHS_638091	Thermo Scientific		
Recombinant DNA reagent	psPAX2	Addgene#12260		
Recombinant DNA reagent	pMD2.G	Addgene#12259		
Recombinant DNA reagent	RHS4346	Thermo Scientific		

Continued on next page

Continued

Reagent type (species) or resource	Designation	Source or reference	Identifiers	Additional information
Recombinant DNA reagent	H$_3$R-shRNA and control-shRNA	This study		See Materials and methods
Sequence-based reagent	RT-qPCR primers	This study		See Materials and methods
Peptide, recombinant protein	TAT-TM peptides	This study		See Materials and methods
Commercial assay or kit	Duolink II in situ PLA detection reagent red Kit	Sigma	Cat. #DUO92008	
Commercial assay or kit	Duolink II PLA probe anti-guinea pig minus	Sigma	Cat. #DUO92010	
Commercial assay or kit	Duolink II PLA probe anti-rabbit plus	Sigma	Cat. #DUO92002 RRID:AB_2810940	
Commercial assay or kit	High Capacity cDNA Reverse Transcription Kit	Applied Biosystems	Cat. #4368814	
Commercial assay or kit	Amplified Luminiscent Proximity Homogeneous Assay kit	AlphaScreen *SureFire* p-ERK 1/2 (Thr202/Tyr204) Assay Kits PerkinElmer	Cat. # TGRESB	
Commercial assay or kit	[^{3}H] SCH 23390	PerkinElmer	Cat. # NET930	0.02 nM to 10 nM
Commercial assay or kit	[^{3}H] R-α-methyl histamine	Perkinelmer	Cat. # NET1027	0.1 nM to 20 nM
Commercial assay or kit	SB 203580	Tocris	Cat. # 1402	1 μM; 10 μM (see Materials and methods)
Commercial assay or kit	SKF 81297	Tocris	Cat. # 1447	100 nM; 1 μM; 30 μM; 50 μM (see Materials and methods)
Commercial assay or kit	SCH 23390	Tocris	Cat. # 0925	one to 50 μM (see Materials and methods)
Commercial assay or kit	Thioperamide maleate salt	Sigma-Aldrich	Cat. #T123	10 μM (cells) 10 mg/kg (mice)
Software, algorithm	Grafit	Erithacus (http://www.erithacus.com/grafit/)		
Software, algorithm	ImageJ	ImageJ (https://imagej.nih.gov/ij/)	RRID:SCR_003070	
Software, algorithm	SMART junior	Panlab (http://www.panlab.com/panlabWeb/Software/php/displaySoft.php?nameSoft=SMART JUNIOR)	RRID:SCR_012154	
Software, algorithm	GraphPad Prism	GraphPad Prism (https://www.graphpad.com/)	RRID:SCR_015807	Version 6

Human brain slices

Paraffin-embedded *post-mortem* 4 μm-thick brain sections containing caudate-putamen were obtained and provided by the Tissue Bank at Hospital Universitario Fundación Alcorcón (Madrid, Spain) and the Netherlands Brain Bank (Amsterdam, The Netherlands) according to the standardized procedures of both institutions. The samples analyzed were from patients with HD (1 grade 0; 1 grade 1; 2 grade 2; 3 grade 3 and 3 grade four patients) and from age matched controls with no neurological disease (three subjects). All protocols were approved by the institutional ethic committees.

Cell cultures

Mouse striatal wild-type STHdh[Q7] and mutant STHdh[Q111] cell lines were provided by Dr M. Macdonald (Center for Genomic Medicine, Boston, USA) and confirmed by PCR. These conditionally immortalized wild-type STHdh[Q7] and mutant STHdh[Q111] striatal neuronal progenitor cell lines expressing endogenous levels of normal and mutant huntingtin with 7 and 111 glutamines, respectively, have been described previously (*Trettel et al., 2000*). These cells do not exhibit amino-terminal inclusions allowing the study of changes involved in early HD pathogenesis (*Trettel et al., 2000*). Striatal cells were grown at 33˚C in DMEM (Sigma-Aldrich), supplemented with 10% fetal bovine serum (FBS), 1% streptomycinpenicillin, 2 mM L-glutamine, 1 mM sodium pyruvate, and 400 g/ml G418 (Geneticin; Invitrogen).

HEK293 cells were purchased from ATCC and kept below passage 20. Cells were grown in Dulbecco's modified Eagle's medium (DMEM) (Gibco, Paisley, Scotland, UK) supplemented with 2 mM L-glutamine, 100 µg/ml sodium pyruvate, 100 U/ml penicillin/streptomycin, essential medium non-essential amino acids solution (1/100) and 5% (v/v) heat inactivated fetal bovine serum (Invitrogen, Paisley, Scotland, UK) and were maintained at 37˚C in an atmosphere with 5% CO_2. Cells were transiently transfected with the corresponding fusion protein cDNA using Lipofectamine 3000 (Invitrogen, Paisley, Scotland, UK). Both cell lines were routinely test for mycoplasma contamination monthly by PCR.

Animal models of HD

Knock-in mice, with targeted insertion of 109 CAG repeats that extends the glutamine segment in murine huntingtin to 111 residues, and the corresponding littermates having seven glutamine residues were maintained on a C57BL/6 genetic background (*Lloret et al., 2006*). Hdh[Q7/Q111] heterozygous males and females were intercrossed to generate age-matched Hdh[Q7/Q111] heterozygous and Hdh[Q7/Q7] wild-type littermates. Only males were used for all experiments. Hemizigous male mice transgenic for exon 1 of the human huntingtin gene with a greatly expanded CAG repeat (~115 CAG repeats in R6/1 mice and ~160 CAG repeats in R6/2 mice) (*Mangiarini et al., 1996*) and wild-type littermates were used when indicated in proximity ligation assays. Animals were housed under a 12 hr light/dark cycle with food and water ad libitum.

Mouse brain slices preparation

For PLA experiments, 2-, 4-, 6- and 8-month-old Hdh[Q7/Q7] and Hdh[Q7/Q111] mice were deeply anesthetized and immediately perfused transcardially with saline (PBS) followed by 4% paraformaldehyde (PFA)/phosphate buffer. Brains were removed and post-fixed overnight in the same solution, cryoprotected by immersion in 10, 20, 30% gradient sucrose (24 hr for each sucrose gradient) at 4˚C and then frozen in dry ice-cooled methylbutane. Serial coronal cryostat sections (30 µm) through the whole brain were collected in PBS-0.025% azide as free-floating sections and stored at 4˚C until PLA experiments were performed. For cell death determination, Hdh[Q7/Q111] and Hdh[Q7/Q7] mice were killed by cervical dislocation at the age of 4, 5 and 8 months. Mouse brains were rapidly removed and placed in ice-cold oxygenated (O_2/CO_2: 95%/5%) Krebs-HCO_3^- buffer (124 mM NaCl, 4 mM KCl, 1.25 mM NaH_2PO_4, 1.5 mM $MgSO_4$, 1.5 mM $CaCl_2$, 10 mM glucose and 26 mM $NaHCO_3$, pH 7.4). Cerebral hemisferes were split and sliced coronally using a McIllwain chopper (Ted Pella, Inc, California) in sterile conditions. Striatum, cortex and hippocampal slices (300 µm thick) were kept at 4˚C in Krebs-HCO_3^- buffer during the dissection and transferred into a Millicell Insert (Millipore).

Cell death determination in striatal cells and in mouse organotypic slice cultures

Striatal STHdh[Q7] or STHdh[Q111] cells were grown to reach 50% of confluence on 12-well plates containing 3 cm^2-glass coverslips. Medium was then replaced by a new supplemented medium containing 0.5% FBS. Vehicle, SCH 23390, thioperamide or SB 203580 were added at the indicated concentrations to cells and incubated for 1 hr before the addition of D_1R. When TAT-TM peptides were applied to cell cultures, these were added 4 hr before the addition of D_1R agonist. After agonist addition, an additional incubation period of 24 hr was performed. Then cells were washed twice in cold-PBS and fixed with 4% paraformaldehyde for 1 hr at 4˚C. Sample nuclei were stained with Hoechst 1:1000. Stained cells were then washed with PBS and mounted under glass coverslips with

Mowiol. A minimum of 10 fields were taken from each coverslip using a fluorescence microscope and the plugin Image-based Tool for Counting Nuclei for ImageJ was used for the quantification of the total nuclei. In mouse organotypic cultures, brain slices (300 µm thickness, see above) were cultured for 24 hr into a Millicell Insert in Neurobasal medium supplemented with 20% horse serum, 0.5% B27, 2 mM L-glutamine, 100 µg/ml sodium pyruvate, non-essential amino acids solution (1/100) and 100 units/ml penicillin/streptomycin (all supplements were from Invitrogen, Paisley, Scotland, UK) before replacing with fresh medium. Vehicle, SCH 23390, thioperamide were added at the indicated concentrations to organotypic cultures and incubated for 1 hr before the addition of D_1R agonist. TAT-TM peptides were applied to cell cultures 4 hr before the addition of D_1R agonist. After agonist addition, an additional incubation period of 48 hr was performed. Then, 10 µM propidium iodide (PI) was added to organotypic cultures and maintained at 37℃ for 1 hr. Organotypic cultures were washed twice in cold-PBS and fixed with 4% paraformaldehyde for 1 hr at 4℃. Total nuclei were stained with Hoechst 1:1000. The Hoechst stained and PI positive nuclei in organotypic cultures were counted to evaluate cell death in the brain slices. Quantification was performed using Leica SP2 confocal microscope (20x; UV, 561 lasers) and the quantification performed with the program Image-based Tool for Counting Nuclei for ImageJ. Cell death is expressed as the percentage of PI positive cells in the total Hoechst-stained nuclei.

Lentivirus production and cell transduction

Silencing lentiviral vectors were produced by co-transfecting HEK293 producing cellsT with lentiviral silencing plasmids GIPZ Human histamine H3 receptor shRNA (Clone V3LHS_638095 or Clone V3LHS_638091, Thermo Scientific) with packing plasmid psPAX2 and envelope coding plasmid pMD2.G (Addgene#12260 and #12259, respectively) using the calcium phosphate method. For production of control non silencing lentiviral particles the H_3R silencing plasmid were substituted with GIPZ Non-silencing Lentiviral shRNA Control (RHS4346, Thermoscientific). Infectious lentiviral particles were harvested at 48 hr post-transfection, centrifuged 10 min at 900 g to get rid of cell debris, and then filtered through 0.45 µm cellulose acetate filters. The titer of recombinant lentivirus was determined by serial dilution on HEK293T cells. For lentivirus transduction, striatal cells were subcultured to 50% confluence, cells were transduced with H_3R-shRNA-expressing lentivirus obtained with plasmid (Clone V3LHS_638095) or control-shRNA-expressing lentivirus (LV control) at a multiplicity of infection (MOI) of 10 in the presence of polybrene 5 µg/ml. Virus-containing supernatant was removed after 3 hr. Puromycin was added to the culturing media at the final concentration of 1 µg/ml 2 days after infection. 5 days after puromycin selection cells were transduced with the second H_3R-shRNA-expressing lentivirus obtained with plasmid Clone V3LHS_638091 to improve the level of silencing achieved. LV control infected cells were re-infected with control-shRNA-expressing lentivirus. The second infection was carried out as the first one. Cells were tested 72 hr after the second transduction was performed.

RNA and real-time PCR

RNA was extracted using TRIzol Reagent (Molecular Research Center). 10 µg of total RNA were treated with RQ1 RNAse free DNAse (Promega) according to manufacturer instruction. DNAse treated DNA was quantified again and cDNA was synthesized using 2 µg total RNA with a High Capacity cDNA Reverse Transcription Kit; (Applied Biosystems). The mRNAs of actin, H3R and D1R were amplified by real-time (RT)-PCR using 1 µL cDNA and power SYBER green PCR Master Mix (Applied Biosystems) on a 7500 Real Time PCR system (Applied Biosystems). Primer sequences are as follows: MsACT For: ATGAGCTGCCTGACGGCCAGGTCAT, MsACT Rev: TGGTACCACCAGA-CAGCAC TGTGTT, H_3R For: GCAACGCGCTGGTCATGCTC, H_3R Rev: CCCCGGCCAAAGG TCCAACG, D_1R FOR: ACCTCTGTGTGATCAGCGTG, AND D_1R REV: GCGTATGTCCTGCTCAACC T. Thermal cycling conditions for amplification were set at 50℃ for 2 min and 95℃ for 10 min, respectively. PCR denaturing was set at 95℃ for 15 s and annealing/extending at 60℃ for 60 s for 40 cycles. mRNA levels normalized for actin are expressed as fold change relative to control cells. The results were quantified with the comparative C_t method (known as the $2^{-\delta\delta Ct}$ method).

In Situ Proximity Ligation Assays (PLA)

Cells or mouse or human brain slices were mounted on glass slides and treated or not with the indicated concentrations of receptor ligands or TAT-TM peptides for the indicated time. Then, cells or slices were thawed at 4°C, washed in 50 mM Tris-HCl, 0.9% NaCl pH 7.8 buffer (TBS), permeabilized with TBS containing 0.01% Triton X-100 for 10 min and successively washed with TBS. Heteromers were detected using the Duolink II in situ PLA detection Kit (OLink; Bioscience, Uppsala, Sweden) following the instructions of the supplier. A mixture of equal amounts of the primary antibodies: guinea pig anti-D_1R antibody (1/200 Frontier Institute, Ishikari, Hokkaido, Japan) and rabbit anti-H_3R antibody (1:200, Alpha diagnostic, San Antonio, Texas, USA) were used to detect D_1R-H_3R heteromers together with PLA probes detecting guinea pig or rabbit antibodies, Duolink II PLA probe anti-guinea pig minus and Duolink II PLA probe anti-rabbit plus. Then samples were processed for ligation and amplification with a Detection Reagent Red and were mounted using a DAPI-containing mounting medium. Samples were observed in a Leica SP2 confocal microscope (Leica Microsystems, Mannheim, Germany) equipped with an apochromatic 63X oil-immersion objective (N.A. 1.4), and a 405 nm and a 561 nm laser lines. For each field of view a stack of two channels (one per staining) and 9 to 15 Z stacks with a step size of 1 μm were acquired. For PLA with brain slices, after image processing, the red channel was depicted in green color to facilitate detection on the blue stained nucleus and maintaining the color intensity constant for all images. A quantification of cells containing one or more spots versus total cells (blue nucleus) and, in cells containing spots, the ratio r (number of red spots/cell containing spots) were determined, using the Fiji package (http://pacific. mpi-cbg.de/), considering a total of 600–800 cells from 4 to 10 different fields within each brain region from three different mice per group or from three human control subjects, 3 human grade 3 or grade 4 HD patients, 2 grade 0 or grade 1 HD patients or 1 grade 2 HD patient. Nuclei and spots were counted on the maximum projections of each image stack. After getting the projection, each channel was processed individually. The nuclei were segmented by filtering with a median filter, subtracting the background, enhancing the contrast with the Contrast Limited Adaptive Histogram Equalization (CLAHE) plug-in and finally applying a threshold to obtain the binary image and the regions of interest (ROI) around each nucleus. Red spots images were also filtered and thresholded to obtain the binary images. Red spots were counted in each of the ROIs obtained in the nuclei images.

Membrane preparation and radioligand binding

Striatal cells or mouse striatal, cortical or hippocampal tissue were homogenized in 50 mM Tris-HCl buffer, pH 7.4, containing a protease inhibitor mixture (1/1000, Sigma). The cellular debris was removed by centrifugation at 13,000 g for 5 min at 4°C, and membranes were obtained by centrifugation at 105,000 g for 1 hr at 4°C. Membranes were washed three more times at the same conditions before use. Ligand binding was performed with membrane suspension (0.2 mg of protein/ml) in 50 mM Tris–HCl buffer, pH 7.4 containing 10 mM $MgCl_2$, at 25°C. To obtain saturation curves, membranes were incubated with increasing free concentrations of [^{3}H] SCH 23390 (0.02 nM to 10 nM, PerkinElmer, Boston, MO, USA) or [^{3}H] R-α-methyl histamine (0.1 nM to 20 nM, PerkinElmer, Boston, MO, USA) providing enough time to achieve stable equilibrium for the lower ligand concentrations. Nonspecific binding was determined in the presence of 30 μM non-labeled ligand. Free and membrane bound ligand were separated by rapid filtration of 500 μl aliquots in a cell harvester (Brandel, Gaithersburg, MD, USA) through Whatman GF/C filters embedded in 0.3% polyethylenimine that were subsequently washed for 5 s with 5 ml of ice-cold Tris–HCl buffer. The filters were incubated overnight with 10 ml of Ecoscint H scintillation cocktail (National Diagnostics, Atlanta, GA, USA) at room temperature and radioactivity counts were determined using a Tri-Carb 1600 scintillation counter (PerkinElmer, Boston, MO, USA) with an efficiency of 62%. Protein was quantified by the bicinchoninic acid method (Pierce Chemical Co., Rockford, IL, USA) using bovine serum albumin dilutions as standard. Monophasic saturation curves were analyzed by non-linear regression, using the commercial Grafit software (Erithacus Software), by fitting the binding data to the equation previously deduced (equation (3) in *Gracia et al., 2013*.

Immunocytochemistry

Cells (60% confluence) were treated with vehicle or 30 μM SKF 81297 and after 45 min cells were kept at 4°C to block endocytosis/exocytosis, washed twice in cold-PBS, fixed in 4% paraformaldehyde for 15 min and washed with PBS containing 20 mM glycine (buffer A) to quench the aldehyde groups. After permeabilization with buffer A containing 0.05% Triton X-100 for 5 min, cells were washed with buffer A containing 1% bovine serum albumin (blocking solution) for 1 hr and labeled with the primary guinea pig anti-D_1R antibody (1/100, Frontier Institute, Ishikari, Hokkaido, Japan, ON at 4°C), washed with blocking solution, and stained with the secondary goat Alexa Fluor 488 anti-guinea pig antibody (1:100, Jackson Immunoresearch Laboratories, West Grove, PA, USA, 2 hr at RT). Samples were washed twice with blocking solution, once with buffer A and finally with PBS. Nuclei were stained with 1:1000 Hoechst. Cells were mounted with Mowiol and observed in a Leica SP2 confocal microscope.

Signaling in striatal cells

To determine ERK1/2 phosphorylation, cells (35,000/well) were cultured with a non-supplemented medium overnight before pre-treated at 25°C for 20 min with the antagonists and stimulated for an additional 7 min with the indicated agonists. Phosphorylation was determined by alpha-screen bead-based technology using the Amplified Luminescence Proximity Homogeneous Assay kit (PerkinElmer, Waltham, MA, USA) and the Enspire Multimode Plate Reader (PerkinElmer) following the instructions of the supplier. To determine calcium release, striatal cells were transfected with 4 μg of GCaMP6 calcium sensor (*Chen et al., 2013b*) using lipofectamine 3000. After 48 hr, cells were incubated (0.2 mg of protein/ml in 96-well black, clear bottom microtiter plates) with Mg^{+2}-free Locke's buffer pH 7.4 (154 mM NaCl, 5.6 mM KCl, 3.6 mM $NaHCO_3$, 2.3 mM $CaCl_2$, 5.6 mM glucose and 5 mM HEPES) supplemented with 10 μM glycine. When TAT-TM peptides treatment was performed they were added 1 hr before the addition of receptor ligands at the indicated concentration. Fluorescence emission intensity of GCaMP6s was recorded at 515 nm upon excitation at 488 nm on an EnSpire Multimode Plate Reader (PerkinElmer, Boston, MO, USA) for 330 s every 5 s and 100 flashes per well. The fluorescence gain was defined as a delta function of $\Delta F/F(t) = (F(t) - F0)/F0$, where F0 is the average fluorescence intensity in the first six measures from the start of recording and F(t) is the fluorescence intensity at a given time and was expressed in %. To determine p38 phosphorylation, striatal cells (80% confluence) were cultured with a non-supplemented medium 4 hr before the addition of the indicated ligand concentration for the indicated time and were lysed with 50 mM Tris-HCl pH 7.4, 50 mM NaF, 150 mM NaCl, 45 mM β-glycerophosphate, 1% Triton X-100, 20 μM phenyl-arsine oxide, 0.4 mM $NaVO_4$ and protease inhibitor cocktail. Lysates (20 μg protein) were processed for western blot a mixture of a rabbit anti-phospho-p38 MAPK (Thr180/Tyr182) antibody (1:1000, Cell Signaling) and a mouse anti-β-tubulin antibody (1:10,000, Sigma). Bands were visualized by the addition of a mixture of IRDye 680 anti-rabbit antibody (1:10,000, LI-COR Biosciences) and IRDye 800 anti-mouse antibody (1:10,000, LI-COR Biosciences) for 2 hr at room temperature and scanned by the Odyssey infrared scanner (LI-COR Biosciences). Band densities were quantified using the Odyssey scanner software. The level of phosphorylated p38 MAPK was normalized for differences in loading using the β-tubulin band intensities.

Mice thioperamide treatment

Thioperamide maleate salt (Sigma-Aldrich, St. Louis, USA) was prepared fresh daily being dissolved in sterile 0,9% saline (NaCl) in order to deliver a final dose of 10 mg/kg in a final volume of 0.01 ml/g of body weight, as previously described (*Charlier et al., 2013*). The vehicle treatment consisted of an equal volume of saline solution. All injections were given via the intra-peritoneal route (*i.p*). Three *i.p* injections per week were administered to wild-type $Hdh^{Q7/Q7}$ and mutant knock-in $Hdh^{Q7/Q111}$ mice from 5 months of age until 6 months of age (when one cohort of animals was perfused to analyze PLA after behavioral assessment) or until 8 months of age (when a second cohort of animals were perfused to analyze PLA at this more advanced disease stage). A total of 11 saline-$Hdh^{Q7/Q7}$ mice, 10 thioperamide-$Hdh^{Q7/Q7}$ mice, seven saline-$Hdh^{Q7/Q111}$ mice and nine thioperamide-$Hdh^{Q7/Q111}$ mice were treated. For these experiments, a total of 11 saline-$Hdh^{Q7/Q7}$ mice, 10 thioperamide-$Hdh^{Q7/Q7}$ mice, seven saline-$Hdh^{Q7/Q111}$ mice and nine thioperamide-$Hdh^{Q7/Q111}$ mice were treated. Similarly, three *i.p* injections per week were administered to wild-type $Hdh^{Q7/Q7}$ and mutant knock-

in Hdh$^{Q7/Q111}$ mice from 7 months of age until 8 months of age to perform the behavioral studies when the D$_1$R-H$_3$R heteromers were lost. For these experiments, a total of 11 saline-Hdh$^{Q7/Q7}$ mice, 12 thioperamide-Hdh$^{Q7/Q7}$ mice, 10 saline-Hdh$^{Q7/Q111}$ mice and 11 thioperamide-Hdh$^{Q7/Q111}$ mice were treated. All treatments were performed in the afternoon to avoid the stress caused by the treatments during the behavioral assessment. Thus, during behavioral analysis treatments were performed after the evaluation of motor learning or cognitive tasks.

Behavior assays

Accelerating rotarod was performed as previously described (*Puigdellívol et al., 2015*). Animals were placed on a motorized rod (30 mm diameter). The rotation speed gradually increased from 4 to 40 rpm over the course of 5 min. The time latency was recorded when the animal was unable to keep up on the rotarod with the increasing speed and fell. Rotarod training/testing was performed as four trials per day during three consecutive days. A resting period of one hour was left between trials. The rotarod apparatus was rigorously cleaned with ethanol between animal trials in order to avoid odors.

For T-maze spontaneous alternation task (T-SAT), the T-maze apparatus used was a wooden maze consisting of three arms, two of them situated at 180° from each other, and the third, representing the stem arm of the T, situated at 90° with respect to the other two. All arms were 45 cm long, 8 cm wide and enclosed by a 20 cm wall. Two identical guillotine doors were placed in the entry of the arms situated at 180°. In the training trial, one arm was closed (new arm) and mice were placed in the stem arm of the T (home arm) and allowed to explore this arm and the other available arm (old arm) for 10 min, after which they were returned to the home cage. After 5 hr (LTM), mice were placed in the stem arm of the T-maze and allowed to freely explore all three arms for 5 min. The arm preference was determined by calculating the time spent in each arm x 100/time spent in both arms (old and new arm). The T-maze was rigorously cleaned with ethanol between animal trials in order to avoid odors.

Novel object recognition test (NORT) consisted in a white circular arena with 40 cm diameter and 40 cm high. Mice were first habituated to the open field arena in the absence of objects (2 days, 15 min/day). During these two days of habitation, several parameters were measured to ensure the proper habituation of all mice in the new ambient. As a measure of anxiety or motivation behaviors, the distance that each mice rove in the periphery or in the center of the open field arena was measured as the rove distance in the periphery or in the center x 100/the total distance. The same analysis was performed by counting the number of entries in the periphery and in the center as well as the time that each mouse spent exploring the periphery or the center. The total distance that each mice rove during these two days of habituation was also recorded as a measure to evaluate spontaneous locomotor activity. On the third day, two similar objects were presented to each mouse during 10 min (A, A' condition) after which the mice were returned to their home cage. Twenty-four hours later (LTM), the same animals were re-tested for 5 min in the arena with a familiar and a new object (A, B condition). The object preference was measured as the time exploring each object ×100/time exploring both objects. The arena was rigorously cleaned with ethanol between animal trials in order to avoid odors. Animals were tracked and recorded with SMART junior software (Panlab, Spain).

Immunohistochemistry, confocal microscopy and immunofluorescence-positive puncta counting

Saline and thioperamide-treated heterozygous mutant Hdh$^{Q7/Q111}$ and WT Hdh$^{Q7/Q7}$ mice at 6 months of age (n = 3 per group) were deeply anesthetized and immediately perfused transcardially with saline followed by 4% paraformaldehyde (PFA)/phosphate buffer. Brains were removed and postfixed overnight in the same solution, cryoprotected by immersion in 30% sucrose and then frozen in dry ice-cooled methylbutane. Serial coronal cryostat sections (30 μm) through the whole brain were collected in PBS as free-floating sections. Sections were rinsed three times in PBS and permeabilized and blocked in PBS containing 0.3% Triton X-100% and 3% normal goat serum (Pierce Biotechnology, Rockford, IL) for 15 min at room temperature. The sections were then washed in PBS and incubated overnight at 4°C with Spinophilin (1:250, Millipore) antibody that were detected with Cy3 anti-rabbit secondary antibodies (1:200, Jackson ImmunoResearch, West Grove, PA). As

negative controls, some sections were processed as described in the absence of primary antibody and no signal was detected. Confocal microscopy analysis and immunofluorescence-positive puncta counting spinophilin-positive spine-like structures was examined as previously described (*Puigdellívol et al., 2015*). Briefly, the images were acquired with Zeiss LSM510 META confocal microscope with HeNe lasers. Images were taken using a $\times 63$ numerical aperture objective with $\times 4$ digital zoom and standard (one Airy disc) pinhole. Three coronal sections (30 μm thick) per animal (n = 3 per group) spaced 0.24 mm apart containing the motor area M1 or CA1 hippocampus were used. For each slice, we obtained three fields/cortical layer (I, II/III and V) of the M1 area and three fields/CA1 hippocampus (*stratum oriens* and *stratum radiatum*). The number and area of spinophilin-positive puncta were measured using NIH ImageJ version 1.33 by Wayne Rasband (National Institutes of Health, Bethesda, MD). To analyze spinophilin immunolabeling, brightness and contrast of fluorescence images were adjusted so that only punctate fluorescence, but no weak diffuse background labeling was visible. In the article, we use the term 'puncta' and 'cluster' interchangeable to refer to discrete points of protein at the fluorescence microscope. Positive puncta/cluster within a specific field was recognized by identifying the presence of overlapping 10–100 pixels.

Western blot analysis

Saline and thioperamide-treated heterozygous mutant $Hdh^{Q7/Q111}$ and WT $Hdh^{Q7/Q7}$, mice were killed by cervical dislocation at 6 months of age, after behavioral assessment. Brains were quickly removed, dissected, frozen in dry ice and stored at −80°C until use. Protein extraction (n = 5–9 per group, only males) and western blot analysis were performed as previously described (*Puigdellívol et al., 2015*). The primary antibody 1C2 (1:1,000, Millipore) was used. Loading control was performed by reproving the membranes with an antibody to α-actin (1:20,000, MP Biochemicals). ImageJ software was used to quantify the different immunoreactive bands relative to the intensity of the α- actin band in the same membranes within a linear range of detection for the enhanced chemiluminescent kit reagent. Data are expressed as the mean ± SEM of band density.

Statistical analysis

All the results were analyzed using GraphPad Prism software version 6.0. Data were presented as mean ± standard error of the means (SEM). Statistical analysis was performed using the unpaired two-sided Student's *t* test (95% confidence), one-way ANOVA or two-way ANOVA with the Bonferroni's *post hoc* test. Values of p<0.05 were considered statistically significant.

Additional information

Author contributions

David Moreno-Delgado, Conceptualization, Formal analysis, Investigation, Methodology, Performed and analyzed viability, calcium, internalization and organotypic culture experiments, Designed the experiments, analysed the results and wrote the manuscript; Mar Puigdellívol, Conceptualization, Formal analysis, Investigation, Methodology, Data curation, Performed all the treatments in mice, Conducted and analyzed the behavioral tests, Obtained all the tissue samples and prepared tissue slices for PLA, organotypic culture and mRNA experiments, Performed and analyzed western blot experiments and conducted and analysed spinophilin-immureactive experiments, Designed the experiments, analysed the results and wrote the manuscript.; Estefanía Moreno, Investigation, Performed PLA experiments and PLA quantification; Mar Rodríguez-Ruiz, Investigation, Assisted with function and viability experiments in cells and organotypic culture; Joaquín Botta, Investigation, Performed the binding experiments and assisted with calcium and cell death experiments; Paola Gasperini, Investigation, Performed all the shRNA related experiments and conducted and analyzed mRNA experiments; Anna Chiarlone, Investigation, Helped with the R6 and human PLA experiments; Lesley A Howell, Resources, Designed, synthesized and purified the disrupting peptides; Marco Scarselli, Resources, Aided with the cell experiments; Vicent Casadó, Antoni Cortés, Investigation, Performed and analyzed binding experiments; Sergi Ferré, Resources, Aided with the disrupting peptide experiments; Manuel Guzmán, Resources, Funding acquisition, Provided R6 mice samples and all the human samples, Discussed the results and edited the manuscript; Carmen Lluís, Supervision, Designed, supervised experiments, discussed, and helped write the manuscript; Jordi Alberch, Funding acquisition, Aided with the in vivo experiments; Enric I Canela, Resources, Funding acquisition, Aided with the disrupting peptide experiments; Silvia Ginés, Peter J McCormick, Conceptualization, Formal analysis, Supervision, Funding acquisition, Project administration, Conceived the idea, designed, supervised and coordinated the project, analyzed the results, and wrote the manuscript

Author ORCIDs

Mar Puigdellívol (iD) https://orcid.org/0000-0002-9955-3558
Joaquín Botta (iD) https://orcid.org/0000-0001-6450-1267
Jordi Alberch (iD) https://orcid.org/0000-0002-8684-2721
Enric I Canela (iD) https://orcid.org/0000-0003-4992-7440
Silvia Ginés (iD) https://orcid.org/0000-0002-9479-8185
Peter J McCormick (iD) https://orcid.org/0000-0002-2225-5181

Ethics

Animal experimentation: All procedures involving animals were performed in compliance with the National Institutes of Health Guide for the Care and Use of Laboratory Animals, and approved by the local animal care committee of the Universitat de Barcelona (99/01) and Generalitat de Catalunya (99/1094), in accordance with the European (2010/63/EU) and Spanish (RD53/2013) regulations for the care and use of laboratory animals. All protocols involving postmortem human sample were approved by the institutional ethic committees.

Decision letter and Author response
Decision letter https://doi.org/10.7554/eLife.51093.sa1
Author response https://doi.org/10.7554/eLife.51093.sa2

Additional files

Supplementary files

• Supplementary file 1. H_3R and D_1R binding parameters in STHdh^{Q7}, STHdh^{Q111} cells. Striatal cells were homogenized in 50 mM Tris-HCl buffer and ligand binding was performed with membrane suspension (see materials and methods). Binding parameters from saturation and competition curves were obtained using Grafit software by fitting the binding data to the equation previously deduced (equation (3) in *Gracia et al., 2013*. Data are mean ± SEM of experiments performed per triplicate.

• Supplementary file 2. H_3R and D_1R binding parameters in different brain regions from 8-month-old Hdh$^{Q7/Q7}$ and Hdh$^{Q7/Q111}$ mice. Mouse striatal, cortical or hippocampal tissue were homogenized in 50 mM Tris-HCl buffer and ligand binding was performed with membrane suspension (see online methods). Binding parameters from saturation and competition curves were obtained using Grafit software by fitting the binding data to the equation previously deduced (equation (3) in *Gracia et al., 2013*. Data are mean ± SEM of experiments performed per triplicate (n = 6 Hdh$^{Q7/Q7}$ and n = 5 Hdh$^{Q7/Q111}$).

• Supplementary file 3. H_3R and D_1R mRNA expression levels the striatum of 4- and 8-month-old Hdh$^{Q7/Q7}$ and Hdh$^{Q7/Q111}$ mice. RT-PCR was performed in striatal extracts from Hdh$^{Q7/Q7}$ and Hdh$^{Q7/Q111}$ at 4 and 8 months of age as described in materials and methods. Results were normalized to actin gene expression. Data represent mean ± SEM (n = 3–4) of experiments performed in duplicate and are expressed as fold change of wild-type animals. Student's two-tailed *t* test was performed.

• Transparent reporting form

Data availability

All data generated or analysed during this study are included in the manuscript and supporting files.

References

André VM, Cepeda C, Fisher YE, Huynh M, Bardakjian N, Singh S, Yang XW, Levine MS. 2011a. Differential electrophysiological changes in striatal output neurons in Huntington's disease. *Journal of Neuroscience* **31**: 1170–1182. DOI: https://doi.org/10.1523/JNEUROSCI.3539-10.2011, PMID: 21273402

André VM, Fisher YE, Levine MS. 2011b. Altered balance of activity in the striatal direct and indirect pathways in mouse models of Huntington's Disease. *Frontiers in Systems Neuroscience* **5**:46. DOI: https://doi.org/10.3389/fnsys.2011.00046, PMID: 21720523

Arrasate M, Finkbeiner S. 2012. Protein aggregates in Huntington's disease. *Experimental Neurology* **238**:1–11. DOI: https://doi.org/10.1016/j.expneurol.2011.12.013, PMID: 22200539

Baba K, Benleulmi-Chaachoua A, Journé AS, Kamal M, Guillaume JL, Dussaud S, Gbahou F, Yettou K, Liu C, Contreras-Alcantara S, Jockers R, Tosini G. 2013. Heteromeric MT1/MT2 melatonin receptors modulate photoreceptor function. *Science Signaling* **6**:ra89. DOI: https://doi.org/10.1126/scisignal.2004302, PMID: 24106342

Beaulieu JM, Gainetdinov RR. 2011. The physiology, signaling, and pharmacology of dopamine receptors. *Pharmacological Reviews* **63**:182–217. DOI: https://doi.org/10.1124/pr.110.002642, PMID: 21303898

Bonaventura J, Navarro G, Casadó-Anguera V, Azdad K, Rea W, Moreno E, Brugarolas M, Mallol J, Canela EI, Lluís C, Cortés A, Volkow ND, Schiffmann SN, Ferré S, Casadó V. 2015. Allosteric interactions between agonists and antagonists within the Adenosine A2A receptor-dopamine D2 receptor heterotetramer. *PNAS* **112**:E3609–E3618. DOI: https://doi.org/10.1073/pnas.1507704112, PMID: 26100888

Brito V, Giralt A, Enriquez-Barreto L, Puigdellívol M, Suelves N, Zamora-Moratalla A, Ballesteros JJ, Martín ED, Dominguez-Iturza N, Morales M, Alberch J, Ginés S. 2014. Neurotrophin receptor p75(NTR) mediates Huntington's disease-associated synaptic and memory dysfunction. *Journal of Clinical Investigation* **124**:4411–4428. DOI: https://doi.org/10.1172/JCI74809, PMID: 25180603

Cahill E, Pascoli V, Trifilieff P, Savoldi D, Kappès V, Lüscher C, Caboche J, Vanhoutte P. 2014. D1R/GluN1 complexes in the striatum integrate dopamine and glutamate signalling to control synaptic plasticity and

cocaine-induced responses. *Molecular Psychiatry* 19:1295–1304. DOI: https://doi.org/10.1038/mp.2014.73, PMID: 25070539

Calebiro D, Nikolaev VO, Lohse MJ. 2010a. Imaging of persistent cAMP signaling by internalized G protein-coupled receptors. *Journal of Molecular Endocrinology* 45:1–8. DOI: https://doi.org/10.1677/JME-10-0014

Calebiro D, Nikolaev VO, Persani L, Lohse MJ. 2010b. Signaling by internalized G-protein-coupled receptors. *Trends in Pharmacological Sciences* 31:221–228. DOI: https://doi.org/10.1016/j.tips.2010.02.002, PMID: 20303186

Cepeda C, André VM, Yamazaki I, Wu N, Kleiman-Weiner M, Levine MS. 2008. Differential electrophysiological properties of dopamine D1 and D2 receptor-containing striatal medium-sized spiny neurons. *The European Journal of Neuroscience* 27:671–682. DOI: https://doi.org/10.1111/j.1460-9568.2008.06038.x, PMID: 18279319

Cepeda C, Levine MS. 1998. Dopamine and N-methyl-D-aspartate receptor interactions in the neostriatum. *Developmental Neuroscience* 20:1–18. DOI: https://doi.org/10.1159/000017294, PMID: 9600386

Charlier Y, Brabant C, Serrano ME, Lamberty Y, Tirelli E. 2013. The prototypical histamine H3 receptor inverse agonist thioperamide improves multiple aspects of memory processing in an inhibitory avoidance task. *Behavioural Brain Research* 253:121–127. DOI: https://doi.org/10.1016/j.bbr.2013.07.016, PMID: 23867149

Chen L, Bohanick JD, Nishihara M, Seamans JK, Yang CR. 2007. Dopamine D1/5 receptor-mediated long-term potentiation of intrinsic excitability in rat prefrontal cortical neurons: ca2+-dependent intracellular signaling. *Journal of Neurophysiology* 97:2448–2464. DOI: https://doi.org/10.1152/jn.00317.2006, PMID: 17229830

Chen JY, Wang EA, Cepeda C, Levine MS. 2013a. Dopamine imbalance in Huntington's disease: a mechanism for the lack of behavioral flexibility. *Frontiers in Neuroscience* 7:114. DOI: https://doi.org/10.3389/fnins.2013.00114

Chen TW, Wardill TJ, Sun Y, Pulver SR, Renninger SL, Baohan A, Schreiter ER, Kerr RA, Orger MB, Jayaraman V, Looger LL, Svoboda K, Kim DS. 2013b. Ultrasensitive fluorescent proteins for imaging neuronal activity. *Nature* 499:295–300. DOI: https://doi.org/10.1038/nature12354, PMID: 23868258

Dau A, Gladding CM, Sepers MD, Raymond LA. 2014. Chronic blockade of extrasynaptic NMDA receptors ameliorates synaptic dysfunction and pro-death signaling in Huntington disease transgenic mice. *Neurobiology of Disease* 62:533–542. DOI: https://doi.org/10.1016/j.nbd.2013.11.013, PMID: 24269729

de Yebenes JG, Landwehrmeyer B, Squitieri F, Reilmann R, Rosser A, Barker RA, Saft C, Magnet MK, Sword A, Rembratt A, Tedroff J, MermaiHD study investigators. 2011. Pridopidine for the treatment of motor function in patients with Huntington's disease (MermaiHD): a phase 3, randomised, double-blind, placebo-controlled trial. *The Lancet Neurology* 10:1049–1057. DOI: https://doi.org/10.1016/S1474-4422(11)70233-2, PMID: 22071279

Ellender TJ, Huerta-Ocampo I, Deisseroth K, Capogna M, Bolam JP. 2011. Differential modulation of excitatory and inhibitory striatal synaptic transmission by histamine. *Journal of Neuroscience* 31:15340–15351. DOI: https://doi.org/10.1523/JNEUROSCI.3144-11.2011, PMID: 22031880

Fan J, Gladding CM, Wang L, Zhang LYJ, Kaufman AM, Milnerwood AJ, Raymond LA. 2012. P38 MAPK is involved in enhanced NMDA receptor-dependent excitotoxicity in YAC transgenic mouse model of Huntington disease. *Neurobiology of Disease* 45:999–1009. DOI: https://doi.org/10.1016/j.nbd.2011.12.019

Ferrada C, Ferré S, Casadó V, Cortés A, Justinova Z, Barnes C, Canela EI, Goldberg SR, Leurs R, Lluis C, Franco R. 2008. Interactions between histamine H3 and dopamine D2 receptors and the implications for striatal function. *Neuropharmacology* 55:190–197. DOI: https://doi.org/10.1016/j.neuropharm.2008.05.008, PMID: 18547596

Ferrada C, Moreno E, Casadó V, Bongers G, Cortés A, Mallol J, Canela EI, Leurs R, Ferré S, Lluís C, Franco R. 2009. Marked changes in signal transduction upon heteromerization of dopamine D1 and histamine H3 receptors. *British Journal of Pharmacology* 157:64–75. DOI: https://doi.org/10.1111/j.1476-5381.2009.00152.x, PMID: 19413572

Ferrante RJ, Kowall NW, Richardson EP. 1991. Proliferative and degenerative changes in striatal spiny neurons in Huntington's disease: a combined study using the section-Golgi method and calbindin D28k immunocytochemistry. *The Journal of Neuroscience* 11:3877–3887. DOI: https://doi.org/10.1523/JNEUROSCI.11-12-03877.1991, PMID: 1836019

Flores-Hernández J, Cepeda C, Hernández-Echeagaray E, Calvert CR, Jokel ES, Fienberg AA, Greengard P, Levine MS. 2002. Dopamine enhancement of NMDA currents in dissociated medium-sized striatal neurons: role of D1 receptors and DARPP-32. *Journal of Neurophysiology* 88:3010–3020. DOI: https://doi.org/10.1152/jn.00361.2002, PMID: 12466426

Frank S, Ondo W, Fahn S, Hunter C, Oakes D, Plumb S, Marshall F, Shoulson I, Eberly S, Walker F, Factor S, Hunt V, Shinaman A, Jankovic J. 2008. A study of chorea after tetrabenazine withdrawal in patients with Huntington disease. *Clinical Neuropharmacology* 31:127–133. DOI: https://doi.org/10.1097/WNF.0b013e3180ca77ea

Fribourg M, Moreno JL, Holloway T, Provasi D, Baki L, Mahajan R, Park G, Adney SK, Hatcher C, Eltit JM, Ruta JD, Albizu L, Li Z, Umali A, Shim J, Fabiato A, MacKerell AD, Brezina V, Sealfon SC, Filizola M, et al. 2011. Decoding the signaling of a GPCR heteromeric complex reveals a unifying mechanism of action of antipsychotic drugs. *Cell* 147:1011–1023. DOI: https://doi.org/10.1016/j.cell.2011.09.055, PMID: 22118459

Garret C, Carruette A, Fardin V, Moussaoui S, Peyronel JF, Blanchard JC, Laduron PM. 1992. RP 67580, a potent and selective substance P non-peptide antagonist]. *Comptes Rendus De l'Academie Des Sciences. Serie III, Sciences De La Vie* 314:199–204. PMID: 1376187

Giménez-Llort L, Martínez E, Ferré S. 1997. Different effects of dopamine antagonists on spontaneous and NMDA-induced motor activity in mice. *Pharmacology Biochemistry and Behavior* 56:549–553. DOI: https://doi.org/10.1016/S0091-3057(96)00295-X, PMID: 9077595

Ginés S, Paoletti P, Alberch J. 2010. Impaired TrkB-mediated ERK1/2 activation in Huntington disease knock-in striatal cells involves reduced p52/p46 shc expression. *Journal of Biological Chemistry* **285**:21537–21548. DOI: https://doi.org/10.1074/jbc.M109.084202, PMID: 20442398

Giralt A, Puigdellívol M, Carretón O, Paoletti P, Valero J, Parra-Damas A, Saura CA, Alberch J, Ginés S. 2012. Long-term memory deficits in Huntington's disease are associated with reduced CBP histone acetylase activity. *Human Molecular Genetics* **21**:1203–1216. DOI: https://doi.org/10.1093/hmg/ddr552, PMID: 22116937

González S, Rangel-Barajas C, Peper M, Lorenzo R, Moreno E, Ciruela F, Borycz J, Ortiz J, Lluís C, Franco R, McCormick PJ, Volkow ND, Rubinstein M, Floran B, Ferré S. 2012a. Dopamine D4 receptor, but not the ADHD-associated D4.7 variant, forms functional heteromers with the dopamine D2S receptor in the brain. *Molecular Psychiatry* **17**:650–662. DOI: https://doi.org/10.1038/mp.2011.93, PMID: 21844870

González S, Moreno-Delgado D, Moreno E, Pérez-Capote K, Franco R, Mallol J, Cortés A, Casadó V, Lluís C, Ortiz J, Ferré S, Canela E, McCormick PJ. 2012b. Circadian-related heteromerization of adrenergic and dopamine $D_{4\times2084}$ receptors modulates melatonin synthesis and release in the pineal gland. *PLOS Biology* **10**: e1001347. DOI: https://doi.org/10.1371/journal.pbio.1001347, PMID: 22723743

Gracia E, Moreno E, Cortés A, Lluís C, Mallol J, McCormick PJ, Canela EI, Casadó V. 2013. Homodimerization of Adenosine $A_{1\times2081}$ receptors in brain cortex explains the biphasic effects of caffeine. *Neuropharmacology* **71**: 56–69. DOI: https://doi.org/10.1016/j.neuropharm.2013.03.005, PMID: 23523559

Guidetti P, Charles V, Chen EY, Reddy PH, Kordower JH, Whetsell WO, Schwarcz R, Tagle DA. 2001. Early degenerative changes in transgenic mice expressing mutant huntingtin involve dendritic abnormalities but no impairment of mitochondrial energy production. *Experimental Neurology* **169**:340–350. DOI: https://doi.org/10.1006/exnr.2000.7626, PMID: 11358447

Guitart X, Navarro G, Moreno E, Yano H, Cai NS, Sánchez-Soto M, Kumar-Barodia S, Naidu YT, Mallol J, Cortés A, Lluís C, Canela EI, Casadó V, McCormick PJ, Ferré S. 2014. Functional selectivity of allosteric interactions within G protein-coupled receptor oligomers: the dopamine D1-D3 receptor Receptor Heterotetramer. *Molecular Pharmacology* **86**:417–429. DOI: https://doi.org/10.1124/mol.114.093096, PMID: 25097189

Haas HL, Sergeeva OA, Selbach O. 2008. Histamine in the nervous system. *Physiological Reviews* **88**:1183–1241. DOI: https://doi.org/10.1152/physrev.00043.2007, PMID: 18626069

Hao J, Janssen WG, Tang Y, Roberts JA, McKay H, Lasley B, Allen PB, Greengard P, Rapp PR, Kordower JH, Hof PR, Morrison JH. 2003. Estrogen increases the number of spinophilin-immunoreactive spines in the Hippocampus of young and aged female rhesus monkeys. *The Journal of Comparative Neurology* **465**:540–550. DOI: https://doi.org/10.1002/cne.10837, PMID: 12975814

Hasbi A, Perreault ML, Shen MY, Zhang L, To R, Fan T, Nguyen T, Ji X, O'Dowd BF, George SR. 2014. A peptide targeting an interaction interface disrupts the dopamine D1-D2 receptor heteromer to block signaling and function *in vitro* and *in vivo*: effective selective antagonism. *The FASEB Journal* **28**:4806–4820. DOI: https://doi.org/10.1096/fj.14-254037, PMID: 25063849

Hoffner G, Souès S, Djian P. 2007. Aggregation of expanded huntingtin in the brains of patients with Huntington disease. *Prion* **1**:26–31. DOI: https://doi.org/10.4161/pri.1.1.4056, PMID: 19172113

Huntington Study Group. 2006. Tetrabenazine as antichorea therapy in Huntington disease: A randomized controlled trial. *Neurology* **66**:366–372. DOI: https://doi.org/10.1212/01.wnl.0000198586.85250.13

Jakel RJ, Maragos WF. 2000. Neuronal cell death in Huntington's disease: a potential role for dopamine. *Trends in Neurosciences* **23**:239–245. DOI: https://doi.org/10.1016/S0166-2236(00)01568-X, PMID: 10838590

Jose PA, Yu PY, Yamaguchi I, Eisner GM, Mouradian MM, Felder CC, Felder RA. 1995. Dopamine D1 receptor regulation of phospholipase C. *Hypertension Research* **18 Suppl 1**:S39–S42. DOI: https://doi.org/10.1291/hypres.18.SupplementI_S39, PMID: 8529072

Kern A, Albarran-Zeckler R, Walsh HE, Smith RG. 2012. Apo-ghrelin receptor forms heteromers with DRD2 in hypothalamic neurons and is essential for anorexigenic effects of DRD2 agonism. *Neuron* **73**:317–332. DOI: https://doi.org/10.1016/j.neuron.2011.10.038, PMID: 22284186

Komater VA, Buckley MJ, Browman KE, Pan JB, Hancock AA, Decker MW, Fox GB. 2005. Effects of histamine H3 receptor antagonists in two models of spatial learning. *Behavioural Brain Research* **159**:295–300. DOI: https://doi.org/10.1016/j.bbr.2004.11.008, PMID: 15817192

Kononoff Vanhanen J, Nuutinen S, Tuominen M, Panula P. 2016. Histamine H3 receptor regulates sensorimotor gating and dopaminergic signaling in the striatum. *Journal of Pharmacology and Experimental Therapeutics* **357**:264–272. DOI: https://doi.org/10.1124/jpet.115.230771, PMID: 26945087

Kotowski SJ, Hopf FW, Seif T, Bonci A, von Zastrow M. 2011. Endocytosis promotes rapid dopaminergic signaling. *Neuron* **71**:278–290. DOI: https://doi.org/10.1016/j.neuron.2011.05.036

Kreitzer AC, Malenka RC. 2007. Endocannabinoid-mediated rescue of striatal LTD and motor deficits in Parkinson's disease models. *Nature* **445**:643–647. DOI: https://doi.org/10.1038/nature05506, PMID: 17287809

Lawrence AD, Watkins LH, Sahakian BJ, Hodges JR, Robbins TW. 2000. Visual object and visuospatial cognition in Huntington's disease: implications for information processing in corticostriatal circuits. *Brain* **123 (Pt 7**:1349–1364. DOI: https://doi.org/10.1093/brain/123.7.1349, PMID: 10869048

Lee LT, Ng SY, Chu JY, Sekar R, Harikumar KG, Miller LJ, Chow BK. 2014. Transmembrane peptides as unique tools to demonstrate the *in vivo* action of a cross-class GPCR heterocomplex. *FASEB Journal : Official Publication of the Federation of American Societies for Experimental Biology* **28**:2632–2644. DOI: https://doi.org/10.1096/fj.13-246868, PMID: 24599960

Lemiere J, Decruyenaere M, Evers-Kiebooms G, Vandenbussche E, Dom R. 2004. Cognitive changes in patients with Huntington's disease (HD) and asymptomatic carriers of the HD mutation–a longitudinal follow-up study. *Journal of Neurology* **251**:935–942. DOI: https://doi.org/10.1007/s00415-004-0461-9, PMID: 15316797

Levy R, Goldman-Rakic PS. 2000. Segregation of working memory functions within the dorsolateral prefrontal cortex. *Experimental Brain Research* **133**:23–32. DOI: https://doi.org/10.1007/s002210000397, PMID: 10933207

Lloret A, Dragileva E, Teed A, Espinola J, Fossale E, Gillis T, Lopez E, Myers RH, MacDonald ME, Wheeler VC. 2006. Genetic background modifies nuclear mutant huntingtin accumulation and HD CAG repeat instability in Huntington's disease knock-in mice. *Human Molecular Genetics* **15**:2015–2024. DOI: https://doi.org/10.1093/hmg/ddl125, PMID: 16687439

Lohse MJ, Calebiro D. 2013. Cell biology: receptor signals come in waves. *Nature* **495**:457–458. DOI: https://doi.org/10.1038/nature12086, PMID: 23515157

López de Maturana R, Sánchez-Pernaute R. 2010. Regulation of corticostriatal synaptic plasticity by G protein-coupled receptors. *CNS & Neurological Disorders Drug Targets* **9**:601–615. DOI: https://doi.org/10.2174/187152710793361531, PMID: 20632967

Lynch G, Kramar EA, Rex CS, Jia Y, Chappas D, Gall CM, Simmons DA. 2007. Brain-derived neurotrophic factor restores synaptic plasticity in a knock-in mouse model of Huntington's disease. *Journal of Neuroscience* **27**:4424–4434. DOI: https://doi.org/10.1523/JNEUROSCI.5113-06.2007, PMID: 17442827

Macdonald M. 1993. A novel gene containing a trinucleotide repeat that is expanded and unstable on Huntington's disease chromosomes. *Cell* **72**:971–983. DOI: https://doi.org/10.1016/0092-8674(93)90585-E

Mangiarini L, Sathasivam K, Seller M, Cozens B, Harper A, Hetherington C, Lawton M, Trottier Y, Lehrach H, Davies SW, Bates GP. 1996. Exon 1 of the HD gene with an expanded CAG repeat is sufficient to cause a progressive neurological phenotype in transgenic mice. *Cell* **87**:493–506. DOI: https://doi.org/10.1016/S0092-8674(00)81369-0, PMID: 8898202

Mattay VS, Goldberg TE, Fera F, Hariri AR, Tessitore A, Egan MF, Kolachana B, Callicott JH, Weinberger DR. 2003. Catechol O-methyltransferase val158-met genotype and individual variation in the brain response to amphetamine. *PNAS* **100**:6186–6191. DOI: https://doi.org/10.1073/pnas.0931309100, PMID: 12716966

Mestre T, Ferreira J, Coelho MM, Rosa M, Sampaio C. 2009. Therapeutic interventions for symptomatic treatment in Huntington's disease. *Cochrane. Database. Syst. Rev.CD* **8**:CD006456. DOI: https://doi.org/10.1002/14651858.CD006456

Milnerwood AJ, Cummings DM, Dallérac GM, Brown JY, Vatsavayai SC, Hirst MC, Rezaie P, Murphy KP. 2006. Early development of aberrant synaptic plasticity in a mouse model of Huntington's disease. *Human Molecular Genetics* **15**:1690–1703. DOI: https://doi.org/10.1093/hmg/ddl092, PMID: 16600988

Mochel F, Durant B, Durr A, Schiffmann R. 2011. Altered dopamine and serotonin metabolism in motorically asymptomatic R6/2 mice. *PLOS ONE* **6**:e18336. DOI: https://doi.org/10.1371/journal.pone.0018336, PMID: 21483838

Mohsen A, Yoshikawa T, Miura Y, Nakamura T, Naganuma F, Shibuya K, Iida T, Harada R, Okamura N, Watanabe T, Yanai K. 2014. Mechanism of the histamine H(3) receptor-mediated increase in exploratory locomotor activity and anxiety-like behaviours in mice. *Neuropharmacology* **81**:188–194. DOI: https://doi.org/10.1016/j.neuropharm.2014.02.003, PMID: 24530460

Moreno E, Hoffmann H, Gonzalez-Sepúlveda M, Navarro G, Casadó V, Cortés A, Mallol J, Vignes M, McCormick PJ, Canela EI, Lluís C, Moratalla R, Ferré S, Ortiz J, Franco R. 2011. Dopamine D1-histamine H3 receptor heteromers provide a selective link to MAPK signaling in GABAergic neurons of the direct striatal pathway. *The Journal of Biological Chemistry* **286**:5846–5854. DOI: https://doi.org/10.1074/jbc.M110.161489, PMID: 21173143

Moreno E, Moreno-Delgado D, Navarro G, Hoffmann HM, Fuentes S, Rosell-Vilar S, Gasperini P, Rodríguez-Ruiz M, Medrano M, Mallol J, Cortés A, Casadó V, Lluís C, Ferré S, Ortiz J, Canela E, McCormick PJ. 2014. Cocaine disrupts histamine H3 receptor modulation of dopamine D1 receptor signaling: σ1-d1-h3 receptor complexes as key targets for reducing cocaine's effects. *Journal of Neuroscience* **34**:3545–3558. DOI: https://doi.org/10.1523/JNEUROSCI.4147-13.2014, PMID: 24599455

Muller M, Leavitt BR. 2014. Iron dysregulation in Huntington's disease. *Journal of Neurochemistry* **130**:328–350. DOI: https://doi.org/10.1111/jnc.12739, PMID: 24717009

Navarro G, Quiroz C, Moreno-Delgado D, Sierakowiak A, McDowell K, Moreno E, Rea W, Cai NS, Aguinaga D, Howell LA, Hausch F, Cortés A, Mallol J, Casadó V, Lluís C, Canela EI, Ferré S, McCormick PJ. 2015. Orexin-corticotropin-releasing factor receptor heteromers in the ventral tegmental area as targets for cocaine. *Journal of Neuroscience* **35**:6639–6653. DOI: https://doi.org/10.1523/JNEUROSCI.4364-14.2015, PMID: 25926444

Orsetti M, Ferretti C, Gamalero R, Ghi P. 2002. Histamine H3-receptor blockade in the rat nucleus basalis magnocellularis improves place recognition memory. *Psychopharmacology* **159**:133–137. DOI: https://doi.org/10.1007/s002130100892, PMID: 11862340

Panula P, Nuutinen S. 2013. The histaminergic network in the brain: basic organization and role in disease. *Nature Reviews. Neuroscience* **14**:472–487. DOI: https://doi.org/10.1038/nrn3526, PMID: 23783198

Paoletti P, Vila I, Rifé M, Lizcano JM, Alberch J, Ginés S. 2008. Dopaminergic and glutamatergic signaling crosstalk in Huntington's disease neurodegeneration: the role of p25/cyclin-dependent kinase 5. *Journal of Neuroscience* **28**:10090–10101. DOI: https://doi.org/10.1523/JNEUROSCI.3237-08.2008, PMID: 18829967

Pascoli V, Boer-Saccomani C, Hermant JF. 2009. H3 receptor antagonists reverse delay-dependent deficits in novel object discrimination by enhancing retrieval. *Psychopharmacology* **202**:141–152. DOI: https://doi.org/10.1007/s00213-008-1171-2, PMID: 18493749

Pillot C, Heron A, Cochois V, Tardivel-Lacombe J, Ligneau X, Schwartz JC, Arrang JM. 2002. A detailed mapping of the histamine H(3) receptor and its gene transcripts in rat brain. *Neuroscience* **114**:173–193. DOI: https://doi.org/10.1016/S0306-4522(02)00135-5, PMID: 12207964

Puigdellívol M, Cherubini M, Brito V, Giralt A, Suelves N, Ballesteros J, Zamora-Moratalla A, Martín ED, Eipper BA, Alberch J, Ginés S. 2015. A role for Kalirin-7 in corticostriatal synaptic dysfunction in Huntington's disease. *Human Molecular Genetics* **24**:7265–7285. DOI: https://doi.org/10.1093/hmg/ddv426, PMID: 26464483

Puigdellívol M, Saavedra A, Pérez-Navarro E. 2016. Cognitive dysfunction in Huntington's disease: mechanisms and therapeutic strategies beyond BDNF. *Brain Pathology* **26**:752–771. DOI: https://doi.org/10.1111/bpa. 12432, PMID: 27529673

Rapanelli M, Frick LR, Pogorelov V, Ota KT, Abbasi E, Ohtsu H, Pittenger C. 2014. Dysregulated intracellular signaling in the striatum in a pathophysiologically grounded model of tourette syndrome. *European Neuropsychopharmacology* **24**:1896–1906. DOI: https://doi.org/10.1016/j.euroneuro.2014.10.007

Rapanelli M, Frick LR, Horn KD, Schwarcz RC, Pogorelov V, Nairn AC, Pittenger C. 2016. The histamine H3 receptor differentially modulates Mitogen-activated protein kinase (MAPK) and akt signaling in striatonigral and striatopallidal neurons. *Journal of Biological Chemistry* **291**:21042–21052. DOI: https://doi.org/10.1074/jbc. M116.731406, PMID: 27510032

Reiner A, Albin RL, Anderson KD, D'Amato CJ, Penney JB, Young AB. 1988. Differential loss of striatal projection neurons in Huntington disease. *PNAS* **85**:5733–5737. DOI: https://doi.org/10.1073/pnas.85.15.5733, PMID: 2456581

Robbins TW. 2000. From arousal to cognition: the integrative position of the prefrontal cortex. *Progress in Brain Research* **126**:469–483. DOI: https://doi.org/10.1016/S0079-6123(00)26030-5, PMID: 11105663

Rosas HD, Koroshetz WJ, Chen YI, Skeuse C, Vangel M, Cudkowicz ME, Caplan K, Marek K, Seidman LJ, Makris N, Jenkins BG, Goldstein JM. 2003. Evidence for more widespread cerebral pathology in early HD: an MRI-based morphometric analysis. *Neurology* **60**:1615–1620. DOI: https://doi.org/10.1212/01.wnl.0000065888.88988.6e, PMID: 12771251

Ross CA, Tabrizi SJ. 2011. Huntington's disease: from molecular pathogenesis to clinical treatment. *The Lancet Neurology* **10**:83–98. DOI: https://doi.org/10.1016/S1474-4422(10)70245-3, PMID: 21163446

Ryu JH, Yanai K, Watanabe T. 1994a. Marked increase in histamine H3 receptors in the striatum and substantia nigra after 6-hydroxydopamine-induced denervation of dopaminergic neurons: an autoradiographic study. *Neuroscience Letters* **178**:19–22. DOI: https://doi.org/10.1016/0304-3940(94)90279-8, PMID: 7816330

Ryu JH, Yanai K, Iwata R, Ido T, Watanabe T. 1994b. Heterogeneous distributions of histamine H3, dopamine D1 and D2 receptors in rat brain. *NeuroReport* **5**:621–624. DOI: https://doi.org/10.1097/00001756-199401000-00022, PMID: 8025257

Sajikumar S, Frey JU. 2004. Late-associativity, synaptic tagging, and the role of dopamine during LTP and LTD. *Neurobiology of Learning and Memory* **82**:12–25. DOI: https://doi.org/10.1016/j.nlm.2004.03.003, PMID: 151 83167

Sánchez-Lemus E, Arias-Montaño JA. 2004. Histamine H3 receptor activation inhibits dopamine D1 receptor-induced cAMP accumulation in rat striatal slices. *Neuroscience Letters* **364**:179–184. DOI: https://doi.org/10. 1016/j.neulet.2004.04.045, PMID: 15196671

Semenova MM, Mäki-Hokkonen AM, Cao J, Komarovski V, Forsberg KM, Koistinaho M, Coffey ET, Courtney MJ. 2007. Rho mediates calcium-dependent activation of p38alpha and subsequent excitotoxic cell death. *Nature Neuroscience* **10**:436–443. DOI: https://doi.org/10.1038/nn1869, PMID: 17369826

Simmons DA, Rex CS, Palmer L, Pandyarajan V, Fedulov V, Gall CM, Lynch G. 2009. Up-regulating BDNF with an ampakine rescues synaptic plasticity and memory in Huntington's disease knockin mice. *PNAS* **106**:4906–4911. DOI: https://doi.org/10.1073/pnas.0811228106

Sotrel A, Williams RS, Kaufmann WE, Myers RH. 1993. Evidence for neuronal degeneration and dendritic plasticity in cortical pyramidal neurons of Huntington's disease: A quantitative Golgi study. *Neurology* **43**: 2088–2096. DOI: https://doi.org/10.1212/WNL.43.10.2088

Spires TL, Grote HE, Garry S, Cordery PM, Van Dellen A, Blakemore C, Hannan AJ. 2004. Dendritic spine pathology and deficits in experience-dependent dendritic plasticity in R6/1 Huntington's disease transgenic mice. *European Journal of Neuroscience* **19**:2799–2807. DOI: https://doi.org/10.1111/j.0953-816X.2004.03374. x, PMID: 15147313

Tang Y, Janssen WG, Hao J, Roberts JA, McKay H, Lasley B, Allen PB, Greengard P, Rapp PR, Kordower JH, Hof PR, Morrison JH. 2004. Estrogen replacement increases spinophilin-immunoreactive spine number in the prefrontal cortex of female rhesus monkeys. *Cerebral Cortex* **14**:215–223. DOI: https://doi.org/10.1093/cercor/bhg121, PMID: 14704219

Tang TS, Chen X, Liu J, Bezprozvanny I. 2007. Dopaminergic signaling and striatal neurodegeneration in Huntington's disease. *The Journal of Neuroscience* **27**:7899–7910. DOI: https://doi.org/10.1523/JNEUROSCI. 1396-07.2007, PMID: 17652581

Taylor DM, Moser R, Régulier E, Breuillaud L, Dixon M, Beesen AA, Elliston L, Silva Santos MF, Kim J, Jones L, Goldstein DR, Ferrante RJ, Luthi-Carter R. 2013. MAP kinase phosphatase 1 (MKP-1/DUSP1) is neuroprotective in Huntington's disease via additive effects of JNK and p38 inhibition. *Journal of Neuroscience* **33**:2313–2325. DOI: https://doi.org/10.1523/JNEUROSCI.4965-11.2013, PMID: 23392662

Trettel F, Rigamonti D, Hilditch-Maguire P, Wheeler VC, Sharp AH, Persichetti F, Cattaneo E, MacDonald ME. 2000. Dominant phenotypes produced by the HD mutation in STHdh(Q111) striatal cells. *Human Molecular Genetics* **9**:2799–2809. DOI: https://doi.org/10.1093/hmg/9.19.2799, PMID: 11092756

Vijayraghavan S, Wang M, Birnbaum SG, Williams GV, Arnsten AF. 2007. Inverted-U dopamine D1 receptor actions on prefrontal neurons engaged in working memory. *Nature Neuroscience* **10**:376–384. DOI: https://doi. org/10.1038/nn1846, PMID: 17277774

Viñals X, Moreno E, Lanfumey L, Cordomí A, Pastor A, de La Torre R, Gasperini P, Navarro G, Howell LA, Pardo L, Lluís C, Canela EI, McCormick PJ, Maldonado R, Robledo P. 2015. Cognitive impairment induced by Delta9-tetrahydrocannabinol occurs through heteromers between cannabinoid CB1 and serotonin 5-HT2A receptors. *PLOS Biology* **13**:e1002194. DOI: https://doi.org/10.1371/journal.pbio.1002194

Vonsattel JP, Myers RH, Stevens TJ, Ferrante RJ, Bird ED, Richardson EP. 1985. Neuropathological classification of Huntington's disease. *Journal of Neuropathology and Experimental Neurology* **44**:559–577. DOI: https://doi.org/10.1097/00005072-198511000-00003, PMID: 2932539

Vonsattel JP, DiFiglia M. 1998. Huntington disease. *Journal of Neuropathology and Experimental Neurology* **57**:369–384. DOI: https://doi.org/10.1097/00005072-199805000-00001, PMID: 9596408

Wang H, Chen X, Li Y, Tang TS, Bezprozvanny I. 2010. Tetrabenazine is neuroprotective in Huntington's disease mice. *Molecular Neurodegeneration* **5**:18. DOI: https://doi.org/10.1186/1750-1326-5-18, PMID: 20420689

Wang JQ, Chen Q, Wang X, Wang QC, Wang Y, Cheng HP, Guo C, Sun Q, Chen Q, Tang TS. 2013. Dysregulation of mitochondrial calcium signaling and superoxide flashes cause mitochondrial genomic DNA damage in Huntington disease. *Journal of Biological Chemistry* **288**:3070–3084. DOI: https://doi.org/10.1074/jbc.M112.407726, PMID: 23250749

Whittaker DS, Wang H-B, Loh DH, Cachope R, Colwell CS. 2017. Possible use of a H3R antagonist for the management of nonmotor symptoms in the Q175 mouse model of Huntington's disease. *Pharmacology Research & Perspectives* **5**:e00344. DOI: https://doi.org/10.1002/prp2.344

Wiescholleck V, Manahan-Vaughan D. 2014. Antagonism of D1/D5 receptors prevents long-term depression (LTD) and learning-facilitated LTD at the perforant path-dentate gyrus synapse in freely behaving rats. *Hippocampus* **24**:1615–1622. DOI: https://doi.org/10.1002/hipo.22340, PMID: 25112177